

Facultad de Física
Departamento de Física Atómica, Molecular y Nuclear



VNIVERSITAT
DE VALÈNCIA

TRITIUM: Design, Construction and Commissioning of an In-Water Tritium Detector

Marcos Martínez Roig

PhD in Physics
May 28, 2021

Under the supervision of:

José Díaz Medina
Nadia Yahlali Haddou

*Dedicated to
my family*

Sometimes it is the people no one imagines anything
of who do the things that no one can imagine.

"Alan Turing"

I

Acknowledgements

Al echar la mirada atrás a estos años de trabajo y formación como investigadora, siento que ha habido muchas personas que me han ayudado directa o indirectamente en esta aventura, por lo que no puede faltar este espacio para agradecer la ayuda que he recibido.

Durante estos 4 años han sido muchas las personas que me han ayudado. Espero no dejarme a nadie.

Ver memoria de "Detectores monolíticos y sensores compatibles con altos campos magnéticos para tomografía por emisión de positrones"

AGRADECER A:

- Gente de tritium Valencia: PEPE, NADIA, MIREIA, ANA, MARQUITOS, ANDREA.
- Gente del LARAM -> TERESA, VANESA, ROSA, CLODO
- Gente de Tritium -> GENTE DE PORTUGAL, Antonio y Jose Angel de extremadura, gente de francia...
- Gente que ha aportado al trabajo:
 - Gente de DUNE (Anselmo, Miguel, Justo)
 - Gente de NEXT (Vicente, Marc, Javier, la chica, etc...)

- Ingeniero electrónico David Calvo del IFIC
 - Gente del IFIMED (Ana Ros, Jhon Barrio y Gabriela Llosa del IFIMED, Rita, Jorge, Marina)
 - Gente de Espectrometría Gamma (El hombre y su mujer, Cesar, Ion, el doctorado, etc)
 - Gente de ATLAS (Urmila, Carlos Mariñas)
 - Gente del ICMOL (El que manda, Lidon)
 - Departamento de mecánica del IFIC (Manolo "Apellidos", Jose Luis Jordan, Jose Vicente Civera Navarrete, Tchogna Davis, Daniel)
 - departamento de electrónica del IFIC (Jorge Nacher Arándiga, Manu ... y el otro)
 - Al departamento de informática (gente)
- Gente externa que ha ayudado
 - DAVID CANAL DE SAMTEC
 - A LUIS FERR... DE PETSYS..
 - Gente externa que no ha ayudado
 - Grupo de amigos del IFIC (nombrar a todos, tanto en el master como en el doctorado)
 - Familia
 - Amigos del pueblo
 - Al programa interreg sudoe -> Soporte financiero!

A carlos por todo su trabajo aportado a esta tesis (TRITIUM-Aveiro 0 prototype and simulations)

Abstract

Tritium is one of the most abundantly emitted radioisotopes in a nuclear power plant. Large quantities of tritium are normally produced in the water of their cooling system, which are finally emitted to the environment. Due to the fact that high quantities of tritium could be dangerous for human health and for the environment, there exist several normative around the world which try to control this radioactive emissions in each country, like the Directive Europeen 2013/51/Euratom, which establishes the tritium limit in drinking water in Europe to 100 Bq/L, or the U. S. Environmental Protection Agency, in United States, whose tritium limit in drinking water is established at 740 Bq/L.

Nowadays, due to such a low energy emitted in the tritium decay, high sensitive detectors are needed for measuring it like LSC. The problem with LSC is that it is an off-line method the measurement process of which can take up to 3 or 4 days, too much time if there are any problem with the NPP.

Detectors based on solid scintillators is a promissing idea for building a tritium detector that works in quasi-real time. This type of detectors has been developed so far succesfully but without achieving enough sensibility for measuring the legal limits.

In this study the results of TRITIUM project is presented. In the

framework of this project a quasi-real time monitor for low tritium activities in water have been developed . This monitor is based on a tritium detector that contains several detection cells which are read in parallel, several active vetos and a pasive shielding for reducing the natural background of our system and an ultrapure water system to prepare the sample before being measured. Each detection cell is made up of hundreds of scintillating fibers read out by PMTs or SiPM arrays.

The final objective of this monitor will be the radiological protection around the nuclear power plant. This monitor will provide an alarm in case of an unexpected tritium release. It will be included in the early alarm system of Extremadura consisting of several detectors the objective of which is to reduce the impact of Nuclear Power Plants to the environment.

Keywords: Tritium in water, Real-time monitor, Nuclear Power Plant, Environmental Safety, ...

Nomenclature and Acronyms

Acronyms:

<i>ICRU</i>	— International Commission of Radioactivity Units and Measurements
<i>ICRP</i>	— International Commission on Radiological Protection
<i>ISR</i>	— International Society of Radiology
<i>UNSCEAR</i>	— United Nations Scientific Committee on the Effects of Atomic Radiation
<i>IAEA</i>	— International Atomic Energy Agency
<i>UN</i>	— United Nations
<i>EU</i>	— European Union
<i>EURATOM</i>	— European Atomic Energy Community
<i>CSN</i>	— Nuclear Safety Council
<i>REA</i>	— Network of automatic stations
<i>REM</i>	— Network of sampling stations
<i>quasi-real</i>	— Less than 10 minutes
<i>LSC</i>	— Liquid Scintillation Counting
<i>PMT</i>	— PhotoMultiplier Tub
<i>SiPM</i>	— Silicon PhotoMultiplier
<i>NPP</i>	— Nuclear Power Plants
<i>U.S.DOE</i>	— United States Department of Energy
<i>U.S.</i>	— United States
<i>PWR</i>	— Pressurized Water Reactor

<i>BWR</i>	— Boiled Water Reactor
<i>HWR</i>	— Heavy Water Reactor
<i>GCR</i>	— Gas-Cooled Reactor
<i>USA</i>	— United States of America
<i>LARAM</i>	— Laboratorio de Radiactividad Ambiental
<i>WHO</i>	— World Health Organization
<i>ALARA</i>	— As Low As Reasonably Achievable
<i>GL</i>	— Guideline
<i>EPA</i>	— Environmental Protection Agency
<i>LDL</i>	— Lower Detection Limit
<i>IC</i>	— Ionization Chamber
<i>BIXS</i>	— Beta Induced X-ray Spectrometry
<i>SDD</i>	— Silicon Drift Detector
<i>APD</i>	— Avalanche Photodiode
<i>EEC</i>	— European Economic Community
<i>CNRS</i>	— Le Centre National de la Recherche Scientifique, France
<i>PMMA</i>	— Polymethyl Methacrylates
<i>CCD</i>	— Charge-Coupled Device
<i>HV</i>	— High Voltage
<i>QE</i>	— Quantum Efficiency
<i>CE</i>	— Collection Efficiency
<i>MPPC</i>	— Multi-Pixel Photon Counter
<i>G – APD</i>	— Geiger Avalanche Photodiode
<i>SSPM</i>	— Solid State PhotoMultiplier
<i>MRS – ADP</i>	— Metal-Resistor-Semiconductor Avalanche Photodiode
<i>MAPD</i>	— Micro-Pixel Avalanche Photodiode
λ	— Wavelength
λ_p	— Maximum wavelength of the associated spectrum
<i>PDE</i>	— Photodetection Efficiency of the SiPM
<i>C_t</i>	— Terminal Capacitance of the SiPM
<i>G_{SiPM}</i>	— Gain of the SiPM

V_{BR}	— Breakdown Voltage of the SiPM
ΔTV_{op}	— Temperature Coefficient (mV/ $^{\circ}C$)
q_e	— Electron Charge
σ_T	— Total Uncertainty of the Measurement
σ_{st}	— Stadistical Component of the Uncertainty
σ_{si}	— Sistematically Component of the Uncertainty
A_m	— Activity Measured
$10 \mu\text{Sv}/\text{cm}$	— MicroSievert per Centimeter
$HPGe$	— High Purity Germanium Detector
ROI	— Region of interest
$PHWR$	— Pressurized Heavy Water Reactor
UDL	— Upper Detection Limit
LWR	— Liquid Water Reactor

Atomic and nuclear symbols

${}_1^1\text{H}$	— Hydrogen
${}_1^2\text{H}$	— Deuterium (Non-Radiactive Hydrogen Isotope)
${}_1^2\text{D}$	— Deuterium (Non-Radiactive Hydrogen Isotope)
${}_1^3\text{H}$	— Tritium (Radiactive hydrogen Isotope)
${}_1^3\text{T}$	— Tritium (Radiactive hydrogen Isotope)
${}_6^{14}\text{C}$	— Carbon
${}_{19}^{40}\text{K}$	— Potassium
${}_{86}^{226}\text{Ra}$	— Radon
${}_2^3\text{He}$	— Isotope of the Helium(Non-radiactive, 1 neutrons)
${}_7^{14}\text{N}$	— Nitrogen
${}_6^{12}\text{C}$	— Carbon
${}_3^6\text{Li}$	— Lithium Isotope
${}_3^7\text{Li}$	— Lithium
${}_5^{10}\text{B}$	— Boron
${}_8^{16}\text{O}$	— Oxygen

X

$^{222}_{86}\text{Rn}$	— Radon
$^{40}_{19}\text{K}$	— Potassium
$^{137}_{55}\text{Cs}$	— Cesium
n	— Free Neutron
H_2O	— Usual Water
D_2O	— Heavy Water
HT	— Air tritium molecule
HTO	— Water tritium molecule
OBT	— Organic tritium molecule
$T_{1/2}$	— Half-life Time of a Radioactive Element
β	— Beta Decay
$\bar{\nu}_e$	— Electron Antineutrino
e^-	— Electron
γ	— Gamma
σ	— Cross Section of a radioactive process
η_{det}	— Intrinsic Detector Efficiency
F_{sci}	— Active surface of the Plastic Scintillator
ε_{det}	— Specific Detector Efficiency
mip	— Minimum Ionizing Particle
Q_β	— Energy released in a radioactive decay
S	— Specific Energy Lost
Z	— Atomic number
$E_\gamma = h\nu$	— Energy of a photon
E_e	— Energy of a electron
m_0	— Rest mass of a electron
c	— Speed of the light in the vacumm
E_b	— Binding Energy
S_{ij}	— Single states of energy levels of electrons in scintillator
T_{ij}	— Triple states of energy levels of electrons in scintillator

Units:

mSv/yr	— Millisievert per Year
mrem	— Millirem
STP	— Standard Temperature ($0^\circ\text{C} = 273\text{K}$) and Pressure (1 atm)
W	— Watt
h	— Hour
$\text{g CO}_2/\text{kWh}$	— Grams of CO_2 per Kilowatt Hour
L	— Liter
Bq	— Becquerel, Nuclear Decay Number per Second
Bq/L	— Becquerel per Liter
Ci	— Curies
Ci/L	— Curies por Liter
yr	— Year
Ci/yr	— Curies per year
GW	— GigaWatt
$\mu\text{S/cm}$	— MicroSivers per Centimeter
kcps	— Kilo Counts per Second
pF	— picoFarads
A	— Ampere (C/s).
C	— Coulomb.
V	— Voltage.
T	— Temperature ($^\circ\text{C}$).
Vol	— Volume (m^3).

Añadir en un futuro:

$D\&D$	— Decontamination and Decommissioning.
DWS	— Drinking Water Standars
NA	— Numerical Apertures

Contents

Acknowledgements	III
Abstract	V
Nomenclature and acronyms	VII
List of Figures	XXI
List of Tables	XXIV
1 Introduction	1
1.1 Tritium and Nuclear Energy	1
1.2 Tritium Properties and Radiological Hazards	9
1.3 Current Legislation	17
1.4 This thesis	20

2 Tritium Detection Systems	21
2.1 State-of-the-Art	21
2.2 TRITIUM Project	25
3 TRITIUM Design Principles	29
3.1 Detector System Overview	29
3.2 TRITIUM Detector	31
3.2.1 Interaction of Particles with Matter	32
3.2.2 Plastic Scintillators	36
3.2.3 Light Detection in Photosensors	43
3.2.4 Electronic Readout	55
3.3 Ultrapure Water System	67
3.3.1 Introduction to the Water System	67
3.3.2 Water System Set Up	68
3.4 Background Rejection System	70
3.4.1 Passive Shield (Lead)	72
3.4.2 Active Shield (Cosmic Veto)	74
4 TRITIUM Detector R&D	79
4.1 Characetrization of the Scintillating Fibers	80

4.1.1	Conditioning Process	80
4.1.2	Automatic Polishing Machine	80
4.1.3	Characterization of Scintillating Fibers	80
4.1.4	Cleaning Process for Scintillating Fibers	80
4.2	Characterization of the SiPM	80
4.3	Characterization of the Ultrapure Water System	80
4.4	Characterization of the Cosmic Veto	80
5	TRITIUM Monitor Prototypes	81
5.1	Preliminary Prototypes	82
5.1.1	TRITIUM-IFIC 0	82
5.1.2	TRITIUM-IFIC 1	82
5.2	Latest TRITIUM Prototypes	82
5.2.1	TRITIUM-Aveiro 0	82
5.2.2	TRITIUM-IFIC 2	82
5.3	Modular TRITIUM Detector	82
6	Simulations	83
6.1	Geant4 Environment	84
6.2	Description of the Simulations Performed	84

6.2.1	Tritiated Water Source	84
6.2.2	Energy deposition and light output of scintillating fibers	84
6.2.3	Fiber Length	84
6.2.4	Fiber Diameter	84
6.2.5	Tritium-IFIC 2	84
6.2.6	Lead Shielding and Cosmic Veto	84
7	TRITIUM Monitor Results and Discussion	85
7.1	Results from Laboratory measurements	86
7.1.1	Experimental Results of TRITIUM-IFIC 0	86
7.1.2	Experimental Results of TRITIUM-IFIC 1	86
7.1.3	Experimental Results of TRITIUM-Aveiro 0	86
7.1.4	Experimental Results of TRITIUM-IFIC 2	86
7.2	Experimental Results in Arrocampo dam	86
8	Results of the TRITIUM Simulations	87
8.1	Optimization of the TRITIUM Monitor Design	88
8.1.1	Optimization of the Tritiated Water Source	88
8.1.2	Simulation of the Output Light of Scintillating Fibers	88
8.1.3	Optimization of the Scintillating Fiber Length	88

8.1.4	Optimization Scintillating Fiber Diameter	88
8.1.5	Effect of the PMMA windows	88
8.2	Simulation Results of TRITIUM monitor	88
8.2.1	Simulation Results of TRITIUM-IFIC 2	88
8.2.2	Simulation Results of Background Rejection System .	88
9	Conclusions and Prospects	89
 Appendices		
A	Electronical Schemes of PCBs Used for SiPM Characterization	93
B	Ultrapure Water System	95
C	Preparation of Liquid Radioactive Source of Tritium	97
D	Electronic System of TRITIUM-Aveiro 0 prototype	99
Bibliography		101

List of Figures

1.1	Annual average distribution of the radioactive dose received by the population [1]	2
1.2	Networks of automatic and sampling stations managed by the spanish CSN.	5
1.3	Tritium sampling locations around Cofrentes NPP.	11
1.4	Tritium activity levels in surface water around Cofrentes NPP from January 2006 to November 2019. The white points are used for the detection limit and the green points are used for the measured activity, when it is above the detection limit. [9]	12
1.5	Tritium activity levels in groundwater around Cofrentes NPP from January 2006 to November 2019. [9]	13
1.6	Tritium decay	14
1.7	Energy spectrum of tritium electrons [31]	15
2.1	Arrocampo dam, Almaraz NPP and Tajus river	26
3.1	Scheme of the scintillator detector	32

3.2	Domain regions of the three most probable types of interactions of gamma rays with matter. The lines show the values of Z and $h\nu$ where the two neighboring effects are equally likely. [76, 77]	34
3.3	Jablonsky diagram. [76]	37
3.4	Stokes shift. [76]	38
3.5	Emission spectrum of BCF-12 fibers of Saint-Gobain. [78]	41
3.6	How photons are collected in a fiber with single clad. [78]	42
3.7	Scheme of a PMT. [76]	45
3.8	Quantum efficiency spectrum for the PMT used (R8520-406). [81]	46
3.9	Hamamatsu commercial voltage divider electronic circuit. Upper circuit with negative supply and lower circuit with positive supply. [81]	48
3.10	Scheme of a APD and electrical symbol used. [84]	50
3.11	Using persistence on the oscilloscope to show several pulses with different heights. Each height associated with a different number of SiPM pixels lit at the same time.	51
3.12	(Left) Electronic scheme of a SiPM and (right) output current of a SiPM as a function of the reverse voltage. It show that the quenching mechanism is essential for working with SiPMs [89].	52
3.13	Electronic scheme of the electronic voltage divider circuit used for working with PMTs without its internal gain.).	56
3.14	Schemes of the different electronic for measuring with PMTs.	58

3.15 Different situation that can happen when time coincidences with PMTs are done.	61
3.16 Signal amplified and logical gate (input signals of MCA).	62
3.17 Different parts of PETSYS system. [103]	63
3.18 Three PCBs used for the SiPM characterization and LED emission spectrum.	66
3.19 Scheme of water purification system.	68
3.20 Lead Bricks and their arrangement in the lead shielding.	73
3.21 Lead Bricks and their arrangement in the lead shielding.	73
3.22 Cosmic veto and Tritium-IFIC 2 prototype in an aluminum mechanical structure developed by IFIC's mechanical engineering department.	74
3.23 Hard cosmic events detected with the cosmic veto of TRI-TIUM: a) Affecting to the tritium measurement, b) Does not affecting to the tritium measurement.	75
3.24 Hard cosmic muon rate [111].	76
3.25 Emission energy spectrum of the plastic scintillation used for the cosmic vetos. [112]	77
3.26 Different layers used to cover of the cosmic veto.	78

List of Tables

1.1	Annual average distribution of the effective dose received by the population due to natural radioactive [2, 3].	3
1.2	Emission of tritium per year from different types of nuclear reactors. Pressurized Water Reactor (PWR), Boiled Water Reactor (BWR), Heavy Water Reactor (HWR) and Gas-Cooled Reactor (GCR) [13]	7
1.3	Most common nuclear reactions of artificial tritium production [13]	10
1.4	Penetration depth for decay electron of mean (5, 7 keV) and maximum (18, 6 keV) energies in different media (tritium gas and air at standard conditions of temperature (273 K) and pressure (1 atm), STP, and water) [32]	15
1.5	Legal limit of tritium in drinking water established in each country.	20

2.1	State-of-the-art in the tritium detection for different techniques. This table show the measured quantity, low detection level (LDL) and the sample form for four different techniques, liquid scintillator counting (LSC), ionization chamber (IC), calorimetry and beta induced X-rays spectrometry (BIXS)	22
2.2	Results of different scintillator detector for tritiated water detection. This table shows the efficiency of the detector (η_{det}), its active surface (F_{sci}), its specific efficiency ($\varepsilon_{det} = \eta_{det}/F_{sci}$), defined as its efficiency normalized to its active surface, and its low detection-level (LDL) for each study listed above.	24
3.1	Critical angles asosciated to different interfaces created with polystyrene, $n_0 = 1.6$, and other materials	43
3.2	Properties of BCF-12 fibers from Saint-Gobain Inc. [78]	44
3.3	Characteristics of SiPM S13360-6075 from Hamamatsu Photonics [86].	53
3.4	Classification of natural radioactive series [107, 108].	71
3.5	Properties of plastic scintillators from Epic-Crystals. [112]	77

Chapter 1

Introduction

1.1 Tritium and Nuclear Energy

Radioactivity has been present in the Universe since its inception. It was an important element of the Big Bang¹, which occurred about $14 \cdot 10^9$ years ago. It was also present during the formation of the earth, $4.5 \cdot 10^9$ years ago, which explains why the different layers that make up the earth contain radioactive elements.

Therefore, humanity has been exposed to radioactivity since its origin, whether present in the Earth's crust or in the universe (external natural irradiation). Even the human being himself is radioactive as radioactive elements are contained in the human body such us ${}^3\text{H}$, ${}^{14}\text{C}$ or ${}^{40}\text{K}$, introduced into the body through food or water ingestion or air inhalation (internal natural irradiation). The annual average of the radioactive dose received by the population is presented in Figure 1.1 and Table 1.1.

¹The Big Bang is the most acceptable hypothesis that explains the formation of the universe and its development over time so far.

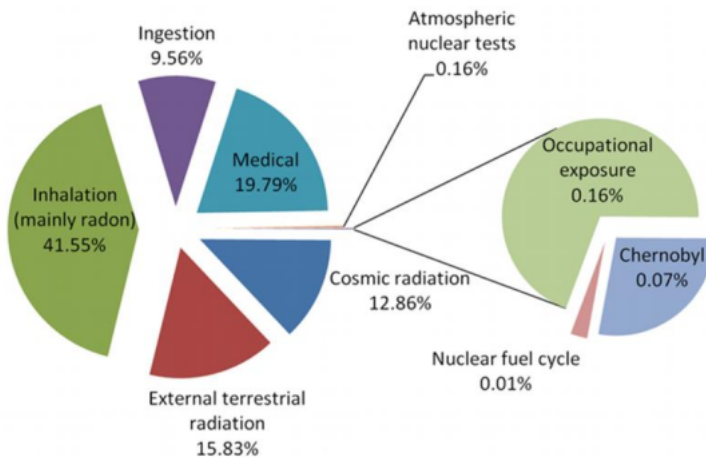


Figura 1.1 – Annual average distribution of the radioactive dose received by the population [1]

As can be seen in Figure 1.1, most of the radioactive dose received by the population is due to both, internal and external natural radiatioactivity, called natural radiation, the effective dose² of which is estimated in 2.42 mSv/yr as can be seen in Table 1.1. It can also be appreciated in Figure 1.1 that the most important part of the artificial radiation received comes from medical treatments.

Since the discovery of radioactivity, made by Hènri Becquerel in 1896, a lot of technology based on nuclear concepts has been developed and applied to several fields such as energy production, research, medicine, industry, etc.

Due to the introduction of radioactivity in the society, various anthropogenic radioactive sources have appeared in the environment, resulting in increased levels of its radioactive elements, called radioactive background.

As our knowledge about radioactivity and our measurement tech-

²The effective dose is the radioactive dose absorbed by the population, taking into account the different radiosensitivity in each organ or tissue.

Radiation source	Eff. dose (mSv/yr)	Typical range (mSv/yr)
Cosmic (external)	0.39	0.3 – 1.0
terrestrial (external)	0.48	0.3 – 0.6
Inhalation (internal)	1.26	0.2 – 10
Ingestion(internal)	0.29	0.2 – 0.8
Total	2.42	1 – 12.4

Table 1.1: Annual average distribution of the effective dose received by the population due to natural radioactive [2, 3].

niques advanced, the negative effects of radioactivity was observed and characterized. Because of that, it is important to control the level of radioactive background to which the population is exposed and to ensure that these levels is kept below of a safe limit. For this task, several organizations were created to forward recommendations in radiological protection to the different organizations and governments of the world.

1. Firstly, a definition of concepts and units was necessary to quantify the negative effects of radioactivity and, for that, the International Commission of Radiological Units and Measurements, ICRU [4], was created during the first international conference of radiology held in London, in 1925.
2. Secondly, the International Commission on Radiological Protection, ICRP [5], was created in 1928 by the International Society of Radiology, ISR [6]. The ICRP aims to make recommendations and to provide guidance on different aspects of protection against radioactivity. The ICRP does not have the legal capacity to enforce its recommendations, but these are widely accepted the legislation of most countries.
3. Thirdly, the United Nations Scientific Committee on the Effects of Atomic Radiation, UNSCEAR [2], was created in 1955, the objective of which is to estimate and report the levels and effects of ionizing

radiation on the population and the environment. These estimates are taken into account by governments around the world to establish their limits and safety standards.

4. Fourthly, the International Atomic Energy Agency, IAEA [1], was created in 1957, which is though to promote the peaceful use of nuclear energy and to avoid its use for any military purpose such us nuclear weapons. Although it is an independent agency, it must to report to the United Nations, UN [7].
5. Fifthly, at the level of the European Union, EU, the European Atomic Energy Community, EURATOM, was created in 1957, which is a international organization established by the EURATOM treaty. Its objective is to coordinate research programs for the peaceful use of nuclear energy and the sharing of knowledge, infrastructure and financing of nuclear energy.
6. Finally, at the national level in Spain, the Nuclear Safety Council, CSN for its acronym in Spanish, was created in 1980 [3]. The CNS is the only institution in Spain in matter of nuclear safety and radiological protection and its objective is to reduce to the maximum the radioactivity in the environment due to anthropogenic origins.

For this task, the CSN has created a number of networks consisting of several detectors of radioactivity that are in charge of controlling the levels of radioactivity in the environment and checking the impact of radioactivity facilities to it. Two of the most important networks are the network of automatic stations and network of sampling stations:

- (a) On the one hand, the network of automatic stations [8], REA for its acronym in Spanish, shown in Figure 1.2a, which consists of several gamma detectors³ distributed in Spain that measure the radioactive dose in real time. The REA is used for the immediate

³Detectors that only measure gamma radioactivity



(a) Measured points of the REA [8]. The white box is the daily average of the gamma dose and the green box is the monthly average of the gamma dose.



(b) Measured points of the REM [9]. Blue dots are located around nuclear facilities. Green dots are uniformly distributed in Spain.

Figura 1.2 – Networks of automatic and sampling stations managed by the spanish CSN.

detection of radiological problems and the application of quick response.

- (b) On the other hand, the network of sampling stations [9], REM for its acronym in Spanish, shown in Figure 1.2b, which consists of several interesting points in Spain where samples are taken and transported to a laboratory to be measured. About twenty Spanish laboratories are integrated into this network, the objective of which is to characterize the concentration and evolution of various radioisotopes present in the radioactive background of Spain and to quantify the impact of radioactive facilities on the environment.

There are other networks that measure different parameters such as the concentration of ^{226}Ra in the air and the measurements of all the networks are adapted to the EUROTAM treaty [10].

The goal of this thesis and the *TRITIUM* project is to develop a monitor capable of automatically measuring low levels of tritium in water in quasi-real time⁴. This monitor is destined to be finally included in the REA.

Tritium is one of the radioactive isotopes routinely measured in REM tests and it is detected through the low-energy electrons produced in tritium beta decay, mainly through the liquid scintillation counter technique, LSC. Due to the limitations of the current methods, which will be shown in section 2.1, the objective of the *TRITIUM* project is to build a tritium detector based on scintillating fibers that will be put directly in contact with the sample (water). The photons produced in these scintillating fibers will be read out using photosensors, either photomultiplier tubes (PMTs) or silicon photomultipliers (SiPMs).

The *TRITIUM* collaboration is an international group consisting of a consortium of 6 different European institutions of 3 different countries: Portugal, France and Spain. The final emplacement of the *TRITIUM* monitor is the Arrocampo dam, Extremadura, Spain, the water of which is used for the cooling system of the Almaraz fission nuclear power plant, NPP. This detector will be installed 4 km downstream from the Almaraz Nuclear Power Plant.

The monitor will be used to ensure that the tritium levels of the Arrocampo dam water are below of the legal limit specified in the EURATOM treaty [10], which is 100 Bq/L. It will be used indirectly to verify the correct operation of the Almaraz NPP, located 4 km above the river since a malfunctioning of it will produce an increase of the tritium activity.

Tritium is one of the most abundantly produced radioisotope in a NPP, as it was verified in the United States Department of Energy complex,

⁴Quasi-real time is an approximation of real-time measurements. It means a relatively small time, like ten minutes.

(U.S. DOE) [11, 12] and in several research facilities in China [13] and places around them (ground water, surface water and process waste water).

Tritium is usually produced in the water used in the nuclear reactor cooling system of some NPPs. It is produced by neutron capture of deuterium, existing in the heavy water (D_2O), semi-heavy water (HDO) or the deuterium created by neutron capture in usual water (H_2O). All these processes have a large probability to happen due to the huge neutron flux in the nuclear reactor, of the order of $10^{14} \text{ n cm}^{-2}\text{s}^{-1}$ [14]. This tritium is finally released partially or totally to the environment with a quantity that depends on the reactor type as it is shown in Table 1.2. The most common way that tritium is released to the environment is HTO [13].

Reactor type	Gaseous discharge (GBq/y)	Liquid discharge (GBq/y)
PWR	$3.70 \cdot 10^3$	$2.59 \cdot 10^4$
BWR	$1.85 \cdot 10^3$	$3.70 \cdot 10^3$
HWR	$7.40 \cdot 10^5$	$1.85 \cdot 10^5$
GCR	$7.40 \cdot 10^3$	$1.11 \cdot 10^4$

Table 1.2: Emission of tritium per year from different types of nuclear reactors. Pressurized Water Reactor (PWR), Boiled Water Reactor (BWR), Heavy Water Reactor (HWR) and Gas-Cooled Reactor (GCR) [13]

NPPs are operational since more than 60 years and, nowadays, they are essential for providing a large part of the electric power used in the world (more than 20% in Spain [15]). Although the Spanish government is planning to progressively shut down all NPP there are other countries like China [16] or United States, USA [17], that promote their use.

On the one hand, NPPs are an interesting investment since it is one of the cheapest source of energy production. It is stable, as it doesn't depend on meteorological parameters and it doesn't emit greenhouse gases. Although there are other alternative energy sources which are being devel-

oped quickly (photovoltaic, wind, tidal energy, etc.), even other concepts of energy production and saving (local production, solar roofs, energy efficiency, smart cities, etc.), today they are not developed enough to fully cover the population needs. On the other hand, NPPs still have some problems such as the contamination of fresh water from uranium mining, the nuclear waste produced, the nuclear proliferation or the risk of radioactive contamination from accidents as happened in the past: Chernobyl, Fukushima and Three Mile Island [18].

In any case nuclear energy production in the world is not going to stop in the next decade, in fact, it will increase as the United States Energy Information Administration (U.S. EIA) expects [19]. Therefore the development of different types of alarm systems is a good investment. Safety is not a negotiable aspect and there must be mechanisms that warn us of any malfunction of a nuclear power plant.

In addition, it is important to highlight that the developed monitor could be used to verify the correct operation of a nuclear power plant, but it is not our objective. Our much broader objective is to ensure that the levels of tritium in the analyzed water are below the Spanish legal limit. It means that this monitor could be used in many different places with radioactive facilities like the future fusion power plants⁵, nuclear research facilities⁶ or tracking the pathway of tritium discharges to ground water [22].

⁵The International Thermonuclear Experimental Reactor, ITER, will need up to several tens of kilograms of tritium to function, which correspond to various TBq of tritium.

⁶Tritium is one of the main emissions from these sites [20], [21].

1.2 Tritium Properties and Radiological Hazards

Tritium is the only radioactive isotope of hydrogen present in the environment. It was for the first time produced in 1934 from neutron capture of deuterium by Ernest Rutherford, Mark Oliphant and Paul Harteck [23] and it was first time isolated in 1939 by Luis Walter Alvarez and Robert Cornog [24], who checked that tritium is a radioactive element.

Tritium is naturally produced in the environment through the interaction of cosmic rays and gaseous elements of the upper atmosphere like nitrogen ($^{14}\text{N}(\text{n}, ^3\text{H}) ^{12}\text{C}$) [25] and oxygen ($^{16}\text{O}(\text{n}, ^3\text{H}) ^{14}\text{N}$) [26]. Around 99% of cosmogenic tritium forms water (HTO) and reaches the Earth's surface as rain with an estimated production rate of $4 \cdot 10^6 \text{ Ci/yr}$ ($1.48 \cdot 10^8 \text{ GBq/yr}$), producing a tritium concentration of $0.6 - 1.2 \text{ Bq/L}$ in precipitation [13, 25].

Tritium can be produced artificially in the environment from different anthropogenic sources [13, 25]. There is a large amount of tritium which was produced in military nuclear test explosions between 1945 and 1975, with an estimated total production of $8 \cdot 10^9 \text{ Ci}$ ($2.96 \cdot 10^{11} \text{ GBq}$) and a part of which remains to the date. In these nuclear explosions, tritium was produced mainly from the nuclear reactions $^{14}\text{N}(\text{n}, ^3\text{H}) ^{12}\text{C}$ and $^2\text{H}(\text{n}, \gamma) ^3\text{H}$. Tritium can also be produced by commercial producers of radioluminescent and neutron generator devices ($1 \cdot 10^6 \text{ Ci/yr}$), nuclear power and defense industries (around $2 \cdot 10^6 \text{ Ci/yr}$) and several research facilities and nuclear reactor for energy production ($2 \cdot 10^6 \text{ Ci/GWyr}$), through the production cross sections shown in Table 1.3:

Tritium levels in the environment excluding anthropogenic radioactive sources are between 1 and 4 Bq/L, larger than the expected due to the cosmogenic background levels ($0.6 - 1.2 \text{ Bq/L}$, previously mentioned) [27]. It can be explained by the consequences of nuclear weapons tests.

Source	Origin	Nuclear reaction	Cross section (b)
^2_1H	Water coolant	$^2_1\text{H}(\text{n}, \gamma)^3_1\text{H}$	$5.2 \cdot 10^{-4}$
^3_2He	Helium coolant	$^3_2\text{He}(\text{n}, \text{p})^3_1\text{H}$	5330
^6_3Li	Moderator	$^6_3\text{Li}(\text{n}, \alpha)^3_1\text{H}$	940
$^{10}_5\text{B}$	Moderator, control rods	$^{10}_5\text{B}(\text{n}, 2\alpha)^3_1\text{H}$	3835

Table 1.3: Most common nuclear reactions of artificial tritium production [13]

Tritium levels in rivers around a nuclear facility are between 1 and 10 Bq/L and even between 20 and 50 Bq/L at the water discharge site of NPPs [27], where the produced tritium is partially or totally released into the environment, mainly in the HTO water form.

The effect of NPP on tritium levels can be observed from REM date, for example the case of Cofrentes. Cofrentes is the closest nuclear power plant to Valencia, in the measurements of which are involved the LARAM⁷. There, the tritium level is measured in three different places along the Jucar river, marked on the map shown in Figure 1.3. The first place, P1, is located in the river, 6 km upstream from the NPP, the second place, P2, is located 1 km downstream and the third place, P3, is located 5 km downstream. The level of tritium measured in these three locations is shown as a function of the time in Figures 1.4a, 1.4b and 1.4c respectively.

In these figures, the detection limit and the measured activity are shown using white and green dots, respectively. The measured activity is only displayed when it is larger than the corresponding detection limit. The tritium level in the river increases due to the discharge of the NPP and it is diluted again after 4 km downstream, as can be seen from these date.

Two additional measurements of the tritium level in groundwater

⁷The LARAM is a Valencia laboratory specialized in environmental radioactivity measurements



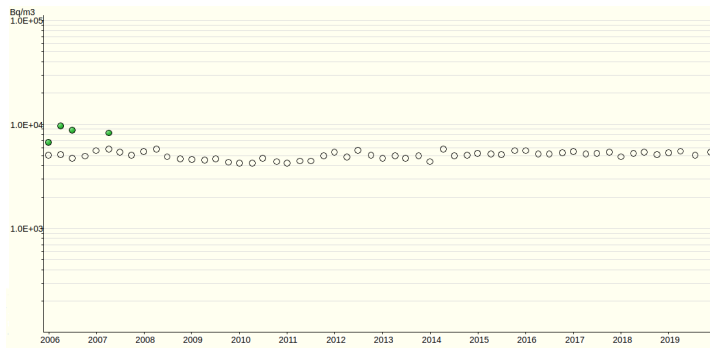
Figura 1.3 – Tritium sampling locations around Cofrentes NPP.

have been included, points S1 and S2 on the map in Figure 1.3, which are located 1 km before and 1 km after the NPP. Both tritium levels are shown in the figure 1.5a and 1.5b respectively, where it can be observed that they are not affected by the nuclear power plant.

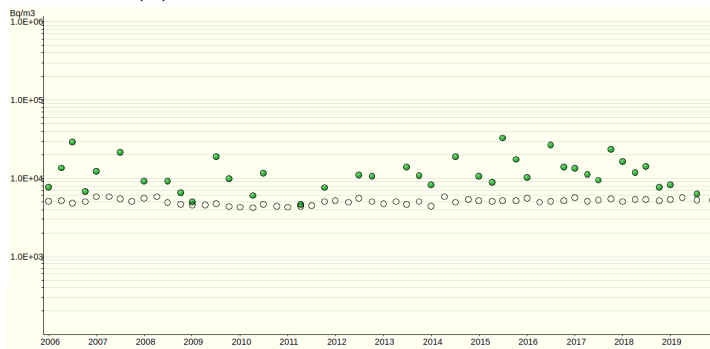
It is important to note that, although environmental tritium level is affected by NPP, these levels are below the maximum allowed limit. The maximum level of tritium measured since of January 2, 2006 is around 32 Bq/L, below to the maximum allowed limit in Europe, 100 Bq/L.

Tritium is a radioactive element with a half-life time of $T_{1/2} = 12.32$ years. It has one proton and two neutrons and decays exclusively through β radiation. It decay 100% directly to the ground state of the ^3_2He isotope of helium, which is a stable nuclei, thorough the decay scheme of equation 1.1:

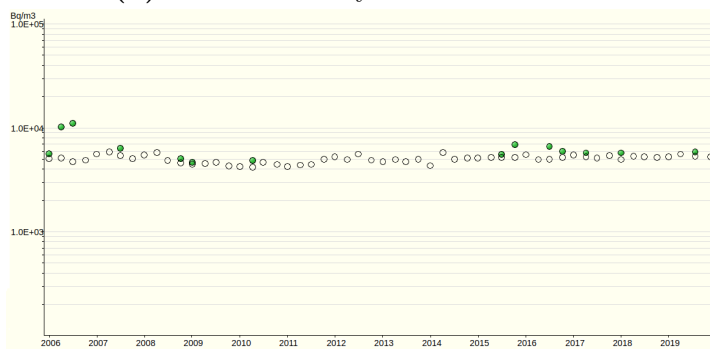




(a) Tritium activity 6 km upstream.

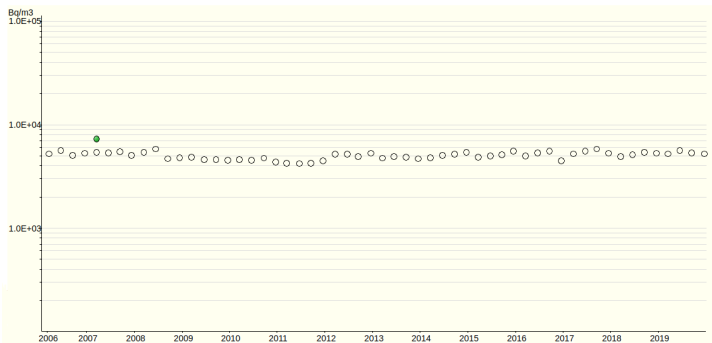


(b) Tritium activity 1 km downstream.



(c) Tritium activity 5 km downstream.

Figura 1.4 – Tritium activity levels in surface water around Cofrentes NPP from January 2006 to November 2019. The white points are used for the detection limit and the green points are used for the measured activity, when it is above the detection limit. [9]

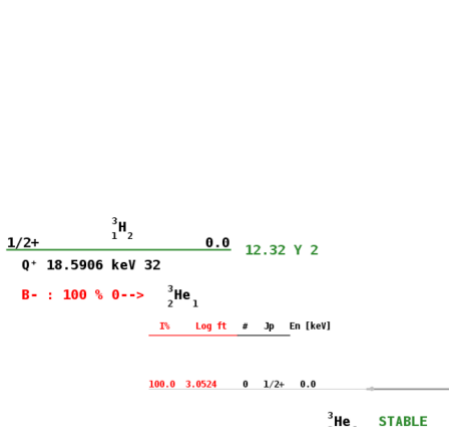


(a) Tritium activity 1 km before NPP.

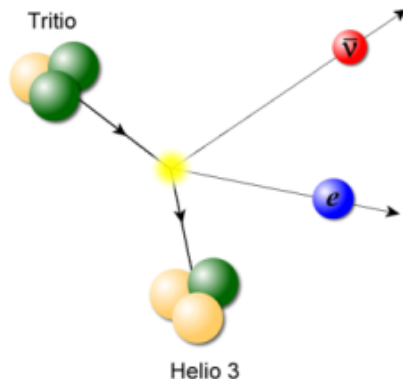


(b) Tritium activity 1 km after NPP.

Figura 1.5 – Tritium activity levels in groundwater around Cofrentes NPP from January 2006 to November 2019. [9]



(a) Tritium energy levels. [29]



(b) Graphic representation of tritium decay [30].

Figura 1.6 – Tritium decay

In Figure 1.6 the scheme of tritium energy levels is shown. In this decay it is not possible to detect the neutrino because of its extremely weak interaction with matter ($\sigma \propto 10^{-42} \text{ cm}^2$ [28]) and, since ^3He has a much larger mass than electrons and neutrinos, by conservation of energy and momentum, the energy that is taken by this daughter nucleus is very small. Therefore, the detection of tritium is through its decay electron.

The energy released in the tritium decay is $Q_\beta = 18.6 \text{ keV}$, shared between the decay products. Therefore, the energy spectrum of the decay electrons is a continuum with a maximum value of 18.6 keV, as shown in Figure 1.7. This energy spectrum has an average energy of 5.7 keV and the most likely energy is slightly below, around 4.5 keV.

The releasing energy of the tritium decay, is very low. In fact, it is the radioactive isotope with the lowest energy released in its β disintegration [25]. Consequently, the β particle which is emitted in this tritium decay will have a very small mean free path, shown in Table 1.4.

This short mean free path is a major issue in tritium detection, as

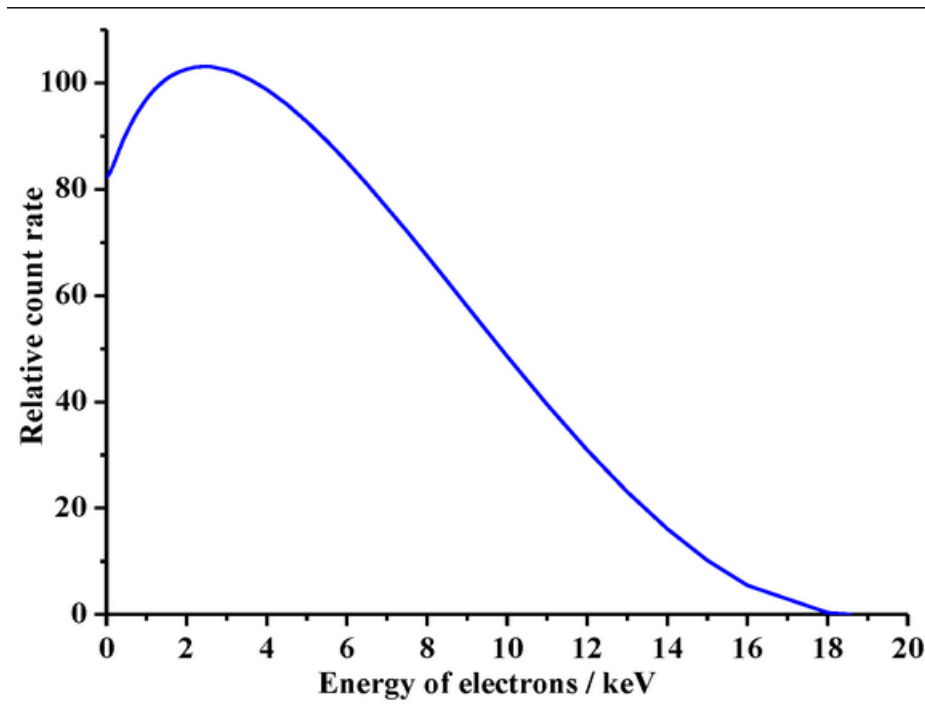


Figura 1.7 – Energy spectrum of tritium electrons [31]

Material	P. Depth (5.7 keV)	P. Depth (18.6 keV)
${}^3_1\text{H}_2$	0.26 cm	3.2 cm
Air	0.036 cm	0.45 cm
Water, soft tissue (solid matter with a density of $1 \text{ g} \cdot \text{cm}^{-3}$)	$0.42 \mu\text{m}$	$5.2 \mu\text{m}$

Table 1.4: Penetration depth for decay electron of mean (5, 7 keV) and maximum (18, 6 keV) energies in different media (tritium gas and air at standard conditions of temperature (273 K) and pressure (1 atm), STP, and water) [32]

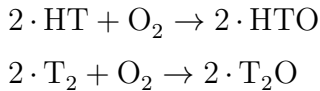
it makes more difficult the electron detection, which will require a highly sensitive detector. It means that tritium electrons have a low penetration in our body and they are easily stopped with clothes or laboratory gloves, resulting in a low radiological hazard of external tritium.

Nevertheless, the danger of tritium increases when it is ingested or inhaled since it can bind anywhere that hydrogen can and perform the same chemical reactions, sometimes with higher rate if the tritium concentration is high enough to catalyze the reaction.

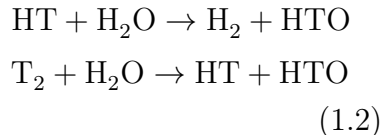
Tritium can be absorbed in our body in three different ways, gaseous tritium (mainly HT), tritiated water (mainly HTO) and organically bound tritium (called OBT).

- The gaseous tritium, which is normally found mixed in the air, is the least important since less than a $3 - 5 \cdot 10^{-3} \%$ is absorbed by the human body, which is insignificant [25]. However, it can be transformed into tritiated water, more harmful from a radiobiological point of interest [25], through the oxidation and exchange reactions by equations 1.2:

Oxidation :



Exchange



- Tritiated water, which is normally found in drinking water and food, has a larger impact since the 99% of it is absorbed [25]. Its biological life time corresponds to the water cycle in the body, around 9.5 days ($\pm 50\%$), time during which tritium will remain in our body [25, 27, 33]. As in water, the biological life time of tritiated water can vary

due to various external parameters such as temperature, humidity, drinking habits, etc. or reduced with the use of diuretics [25].

- Organically bound tritium, normally found in food, generally forms a covalent bond with a carbon and it corresponds to 5 – 10 % of tritium absorbed in the body. Although it is less absorbed in the body than tritiated water, it can be more dangerous since it has a longer biological life time. The biological life time of this tritium type depends on the affinity of the organic molecule to the different biological tissues and it can vary from tens to hundreds of days (larger than the ICRP estimate) [27, 33, 34, 35].

There are many studies showing that tritium in living matter can cause the same effects than X-rays or γ rays, which are mutations, tumors, cancer, genetic effects, reproductive effects, etc [36, 37]. In fact, the consequences of tritium radiation can be worse than a similar γ radiations since its biological efficiency⁸ is two or three times larger [36].

In summary, tritium is a naturally occurring radioactive element that can affect health if it is released excessively. Because of that, each country has developed a legislation, shown in section 1.3, to manage the release of tritium and ensure that these background levels are safe for health.

1.3 Current Legislation

Due to the radiological risk of tritium, which was deal with in section 1.2, it is important that the current legislation limits the release of tritium to the environment ensuring that the levels are below a safe value for health.

⁸The biological efficiency is used to quantify the damage produced in the living cells due to an external radiation.

The guidelines setting impose the limit of radioactive elements in drinking water for many countries are based on the radiation protection methodology developed by the ICRP [38] and the recommendations of the world health organization (WHO) [39].

The objective of the international radiation methodology is to protect people and the environment from the negative effects of ionizing radiations but allowing beneficial activities that involve a reasonable radiation exposure. It is based on three main points, which are the justification (the benefit from radiological exposure must outweigh the detriment to health that it causes), the ALARA principle, "As Low As Reasonably Achievable" (the radiological exposure must be kept as low as possible considering social and economic factors) and dose limitation (limit that must never be exceeded).

While the ICRP recommends a maximum dose of 1 mSv/yr, excluding the natural background and medical interventions, the WHO is more conservative, recommending a maximum dose of 0.1 mSv/yr, which correspond to less than 5% of the annual dose due to background radiation, 2.42 mSv/year, Table 1.1.

The guideline reference level of each radionuclide in drinking water, GL, is usually calculated from these recommendations using the equation

$$GL = \frac{RDL}{DCF \cdot q} \quad (1.3)$$

where RDL is the reference dose level, DCF is the dose conversion factor (the normal used value for tritium is 1.810^{-11} SvBq, provided by ICRP [40]) and q is an estimation of the annual volume of drinking water consumed (normally assumed two liters per day, 730 L/yr).

The GLD calculated for tritium in drinking water according to the ICRP and WHO recommendations is 76,103 Bq/L and 7,610 Bq/L

respectively. It means that tritiated water with activities below these values is considered not harmful to health.

Based on these recommendations, each country has created organizations in charge of developing its own legislation on radionuclide limits. In Spain, the responsible organization of this task is the CSN.

Most of the countries in the world implement the RDL of 0.1 mSv/yr recommended by the WHO. The legal limit for tritium in drinking water in this case is 76,103 Bq/L but it is often approximated in different ways. Some countries like Switzerland [41] or some organizations like the WHO [39] rounded this value to 10,000 Bq/L. Others like some countries of Canada, such as Ontario and Québec, truncate this value to the first number 7,000 Bq/L [42, 43]. There are other countries like Russia which use the much more accurate approximation value of 7,700 Bq/L [44].

There are other countries like Australia that prefer to implement the RDL of 1 mSv/yr, recommended by the ICRP, the legal limit of which is 76,103 Bq/L [45]. Other countries like Finland are based in the ICRP recommendations and use only the middle of this value, 0.5 mSv/yr, the value of which is rounded to a legal limit of 30,000 Bq/L for tritium in drinking water [46].

There are two different exceptions to these recommendations:

1. On the one hand, most of the USA states like California use a RDL of 4 mrem (0.04 mSv), which corresponds to a legal limit of 20 nCi/L (740 Bq/L) [47]. This value was proposed by the United States Environmental Protection Agency (US EPA) as a result of an analysis of the available information [48].
2. On the other hand, most of the EU countries, such as France, Germany or Spain, impose an GL of 100 Bq/L, which is one of the most restrictive limit in the world [49, 50, 51]. This value arise from the

consideration that it is an indicator of the presence of other radionuclides more dangerous than tritium. These limits are fixed by the EURATOM Council Directive [52].

All limits mentioned in this section are summarized in table 1.5.

Country/Agency	Legal limit of tritium (Bq/L)
ICRP	76,103
WHO	10,000
Switzerland	10,000
Canada	7,000
Russia	7,700
Australia	76,103
Finland	30,000
United States	740
European Union	100

Table 1.5: Legal limit of tritium in drinking water established in each country.

1.4 This thesis

Chapter 2

Tritium Detection Systems

2.1 State-of-the-Art

Measurement of tritium activity is one of the routine environmental controls that are carried out in the vicinity of nuclear research facilities and nuclear power plants during their energy production lifetime. Consequently, this measurement has been carried out with different available technologies under development to improve the state of the art of tritium detection. The most employed techniques are summarized in Table 2.1.

Nowadays, the most used technique for measuring tritium in water is liquid scintillator counting (LSC). This technique consists of mixing a liquid sample (some ml for environmental measurements or less for higher activities) with liquid scintillator. This mixture is usually made in a ratio of 50:50 but it depends on the detection system and the samples used [53, 54]. In this technique, the β energy emitted from the sample excites the molecular energy levels of the liquid scintillator which promptly decays emitting several photons with a well-known energy (fluorescence), usually in the visible spectrum. Finally these photons are detected with photosen-

	LSC	IC	Calorimetry	BIXS
Measured quantity	Scintillation photons	Ionization current	heat	X-rays
LDL	\sim Bq	10 – 100 kBq	\sim GBq	\sim MBq
Sample form	Liquid	Gas, vapor	All	All

Table 2.1: State-of-the-art in the tritium detection for different techniques. This table show the measured quantity, low detection level (LDL) and the sample form for four different techniques, liquid scintillator counting (LSC), ionization chamber (IC), calorimetry and beta induced X-rays spectrometry (BIXS)

sors, which convert the optical signal into measurable electrical charge. The liquid scintillator technique has a very good detection sensitivity for low activity levels of tritiated water ($< 1 \text{ Bq/L}$) [55] but it has the problems of long measurement time (up to 2 days) and of producing chemical waste, as liquid scintillator contains toluene which is toxic. In addition, this technique requires special staff for sampling, chain-of-custody and lab analysis which require economical and time resources. In order to avoid this problem some unsuccessful efforts have been made in order to build a monitor of tritium with LSC [56].

The ionization chamber (IC) consists of a gas chamber (sample) which contains electrodes connected to different voltages. These electrodes collect the ionization current that is produced due to the β radiation. It is a simple and fast system, but it has the problem of high Low Detection Limit ($> 10 \text{ kBq}$) and of requiring the samples to be in a state of gas or steam [57, 58].

The calorimetry method is based on the measurement of the heat generated in the detection medium (normally platinum) [59, 60]. The problem with this technique is that it has a high LDL, of the order of GBq, and requires long measurement time, 2 days or more.

The Beta Induced X-ray Spectrometry (BIXS) is based on the measurement of the bremsstrahlung radiation produced by the tritium decay electrons, using a NaI(Tl) crystal couplet to a PMT [61, 62] or Silicon Drift Detector (SDD) [63]. The problem with this technique is a high LDL, of the order of MBq.

There are additional methods for tritium detection, although they are less employed or less experimentally developed, each one with its own advantages and limitations. For example, the Avalanche PhotoDiode (APD) cannot be used in contact with water [64], the mass spectrometry which needs to store the sample several months before taking the measurement [65] and the Cavity ring spectroscopy requires a special optical configuration that is not possible outside a laboratory [66].

All the above techniques are offline methods that need long time for sample collection, shipment to the laboratory and activities measurements. Therefore, they cannot be used for in-situ monitoring of tritium in water. The liquid scintillation technique is the only one with sufficiently small Low-Detection-Limit to fulfill the compliance of 100 Bq/L in tritium of the water samples, established by the EURATOM directive.

The purpose of the TRITIUM project is to develop an alternative method, based on solid scintillators, that allows to accomplish the requirements of in-situ monitoring of levels as low as the legal limit in Europe 100 Bq/L in quasi-real time. There are several studies that have developed with solid scintillators so far:

1. The study done by M. Muramatsu, A. Koyano and N. Tokunaga in 1967 who used a scintillator plate read out by two PMTs in coincidence [67].
2. The study carried out by the A. A. Moghissi, H. L. Kelley, C. R. Phillips and J. E. Regnier in 1969 that used one hundred plastic fibers

coated with anthracene powder and read out by two PMTs in coincidence [68].

3. The study performed by R. V. Osborne in 1969 that used sixty stacked scintillator plates read out by two PMTs in coincidences [69].
4. The study done by A. N. Singh, M. Ratnakaran and K. G. Vohra in 1985, that used a scintillator sponge read out by PMTs in electronic coincidence [70, 71].
5. The study carried out by K. J. Hofstetter and H. T. Wilson in 1991, that tested different shapes of scintillator plastics like several sizes of beads, fibers, etc. The better result obtained for solid plastic scintillator was a tritium detection efficiency of the order of 10^{-3} [72, 73].

Study	$\varepsilon_{det}(\frac{cps \cdot 10^{-3}}{kBq/L})$	F_{sci} (cm ²)	$\eta_{det}(\frac{cps \cdot 10^{-6}}{kBq/L \cdot cm^2})$	LDL (kBq/L)
Muramatsu	0.39	123	3.13	370
Moghissi	4.50	> 424.1	< 10.6	37
Osborne	12	3000	4	37
Singh	41	3000	13.7	< 37
Hofstetter	2.22	~ 100	< 22.2	25

Table 2.2: Results of different scintillator detector for tritiated water detection. This table shows the efficiency of the detector (η_{det}), its active surface (F_{sci}), its specific efficiency ($\varepsilon_{det} = \eta_{det}/F_{sci}$), defined as its efficiency normalized to its active surface, and its low detection-level (LDL) for each study listed above.

The results of these experiments are summarized in Table 2.2. As can be seen, in the first column that the intrinsic detector efficiency, ε_{det} , is very different in these experiments. As one of the most important factor that affect the efficiency is the active surface of the plastic scintillator, F_{sci} , which varies largely with the detector type, the specific detector efficiency (third column) is used in order to compare these experiments, that is, the intrinsic

detector efficiency normalized to this active surface. It can be checked that, effectively, these specific efficiencies are quite similar. The specific efficiency obtained by Moghissi for scintillating fibers is sufficiently high to justify our choice of scintillating fibers as a detection medium. Finally, as can be seen in the last column, the LDL in all these experiments are of the order of a few tens of kBq/L. Thus, to develop a detector which much lower LDL is essential to comply with the EURATOM directive of 100 Bq/L of tritium in water for human consumption.

2.2 TRITIUM Project

As a conclusion of section 2.1, the current techniques cannot be used for tritium monitoring in quasi-real time since they have either a higher LDL or they work in off-line method (too slow).

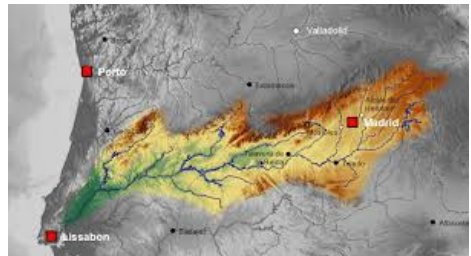
To overcome these limitations the *Tritium* project [74], with the title of "Design, construction and commissioning of automatic stations for quasi-real time monitoring of low radioactive levels of tritium in water", was proposed.

The *Tritium* collaboration is a international group consisting of a consortium of 6 different european institution of 3 different countries: The University of Aveiro, in Portugal, The University of Bordeaux and the National Center for Scientific Research, CNRS (Section Aquitaine-Limousin), in France and the University of Extremadura, *Junta de Extremadura* and University of Valencia, in Spain.

This project was funded by the Interreg Sudoe program of the European Economical Community, EEC, in the 2016 call with the reference number SOE1/P4/EO214. The purpose of this project is the development of a tritium monitor in quasi-real time. This monitor consists of a ultra-



(a) Arrocampo dam and Almaraz Nuclear Power Plant.



(b) Tajus river along Spain and Portugal.

Figura 2.1 – Arrocampo dam, Almaraz NPP and Tajus river

pure water system, which prepare the water sample before introducing it in the detector for tritium measurement, a cosmic veto and a passive shielding, which reduce the natural background of our tritium detector, and several electronic modules which control all the different parts of the monitor, analyze the tritium measurement and send an alarm if the configured limit (100 Bq/L) is exceeded.

A crucial problem is to distinguish tritium signals from the background because tritium events has low energy (\sim keV) and fall in an energy range of the spectrum where there is significant background. To reduce the background counts of TRITIUM monitor, coincidence techniques are used.

The TRITIUM monitor will be installed in the Arrocampo dam, Almaraz, Spain, where the Almaraz NPP release the water of the secondary cooling circuit, displayed in Figure 2.1. This NPP has two nuclear reactors of PWR type. Arrocampo dam is located near the Tagus river, shown in Figure 2.1b, which is the longest river in Spain, with a long of the 1007 km. This river, shown in Figure 2.1a, rises in Aragon (Spain) and flows into the Atlantic Ocean, Lisbon (Portugal). The water of this river is used for agriculture and drinking water by both, Spanish and Portuguese people. Therefore the international cooperation in order to maintain the quality of the tajus river water is very important.

Each institution has concentrated its efforts in the development of a different part of this project:

1. The Extremadura group has developed and installed the ultrapure water system to produce water with very low conductivity, $\sigma \approx 10 \mu\text{Sv}/\text{cm}$ (two orders less than sample before the cleaning process, $1000 \mu\text{Sv}/\text{cm}$). This cleaning process is very important for two reasons. On the one hand, for maintaining our detector very clean, which is a critical point. On the other hand, to reduce the natural background since several natural radioactive isotopes presents in this water (except tritium) are removed such as ^{222}Rn , ^{40}K or ^{137}Cs . This system is explained in section 3.3.
2. The french group has develop the pasive shielding for the detector. The shielding is made of ultra radiopure lead with very low intrinsic activity in order to reduce the external natural background of the system. This shielding is presented in section 3.4.1.
3. The Portuguese and Spanish group have collaborated for designing, developing and building four different prototypes of tritium detector and active vetos for removing cosmic events. These prototypes and vetos are explained in chapter 5 and section 3.4.2 respectively.
4. The Portugal and Spanish people have also carried out simulations of this system. The environment chosen to develop these simulations is the package GEANT4 [75], consisting of an extensive C++ library with which the geometry of our detector, the relevant physical processes, etc. can be designed. This simulation are explained in chapter 6.

The important characteristics of the TRITIUM detector must have:

- *Compact.* This is an important point because in the place where this detector will be installed the useful space to be used is very limited.

- *Thin active volume and large active area.* On the one hand, it have to be taken into account that the mean free path of the β particle of tritium decay is very low so thin detector active volumes are needed. In practice, active thickness beyond the mean free path of the tritium electrons will only contribute to background. On the other hand, as explained in section 2.1, the efficiency of this type of detector scales with the active area, so it is crucial to design the detector with the largest possible active area.
- *High efficiency to tritium.* As the tritium activities to be measured are very low, it is very important to reduce as much as possible the non-detected tritium events.
- *High specificity to tritium.* The detector has to be able to distinguish the tritium signal from the signal due to other radioactive elements present in the sample.
- *Quasi-real time response.* It is important that the sistem work in quasi-real time in order to detect any problem as fast as possible.
- *Rugged system.* Finally, it has to be take into account that the final goal is to install an automatical system which work during a number of years without requiring the intervention of specialized people, which requires a rugged monitor.

In order to get the measurement in quasi-real time it is needed to work *in situ*, that is, in the same place that the water sample is taken. Working *in situ* has some benefits for the detector such as faster and cheaper maintenance since the sampling process, chain of custody, etc. are eliminated, more frequent measurements are carried out and safer monitoring since personal exposure dose is reduced, changes in activity levels can be detected quickly and possible errors due to specialized staff are eliminated.

Chapter 3

Design Principles of the Tritium Monitor

3.1 Detector System Overview

The objective of the TRITIUM project is the design, development, construction and commissioning of an automatic station for real-time monitoring of low levels of tritium in water. To achieve this aim, the TRITIUM group has developed a monitor consisting of several parts, listed below:

1. The TRITIUM detector, described in chapter 5, is based on several modules read in parallel. Each module consists of hundreds of scintillating fibers, section 3.2.2, which are in contact with the water sample measured, read by two coincident photosensors, section 3.2.3. The photosensors are photomultiplier tubes (PMT) (section 3.2.3) and silicon photomultipliers (SiPM) (section 3.2.3).
2. The ultrapure water system (section 3.3) that prepares the water sample before measurement. This system removes all the organic parti-

cles dissolved and all the particles with a diameter greater than $1 \mu\text{m}$ without affecting the tritium content of the sample. This system is important for two reasons: First, because the mean free path of tritium in water is very short, 5 or $6 \mu\text{m}$, so it is essential to avoid the deposition of particles onto the fibers because this would prevent the tritium decay electrons from reaching the fibers. Second, particles dissolved in water may contain radioactive isotopes like ^{40}K , which would increase the background. As the water sample has very low tritium counters, to reduce the background is a crucial matter.

3. The background rejection system (section 3.4), that has two different parts. The first one is a passive shield (section 3.4.1), consisting of a lead castle inside of which the TRITIUM detector is located. This castle is employed to eliminate natural radioactive background and cosmic rays with energies of the order of 200 MeV/nucleon . The second part is an active veto (section 3.4.2), consisting of two plastic scintillation blocks located inside of a passive shielding, above and below the TRITIUM detector and read by several photosensors. The goal of this active veto is to remove the remaining high energy events ($> 200 \text{ MeV}$) cosmic rays that can travel through the passive shielding and contribute to background. Contrary to low energy cosmic rays, high energy cosmic rays are difficult to be stopped. The technique employed to eliminate their contribution consists of reading the TRITIUM detector in anti-coincidence with the active veto.
4. A monitoring electronic system sends an alarm if the signal limit of the tritium level, 100 Bq/s , is exceeded.

The different parts of TRITIUM monitor were subjected to tests to verify their correct operation before installing them in the Arrocampo dam. The final goal is to include TRITIUM in the network of automatic stations, REA (section 1.1).

3.2 TRITIUM Detector

As discussed in section 2.1, the TRITIUM consists in a chain of three main elements:

- The scintillator, that detects the tritium event, as ionizing radiation hits this material and deposits kinetic energy through ionization and excitation processes, part of the absorbed energy is converted in to photons, mostly in the visible range¹. The produced photons carry information about the particle detected, like its energy, type, etc.
- The photosensor, that detects the photons produced in the scintillator. The most common photosensors in nuclear physics are PMTs and SiPMs. They detect the photons produced in the scintillator with an efficiency and transforms them in electrons with a multiplication factor of around 10^6 . These electrons form a electronic pulse than gives information of the detected photons.
- The electronic system, which is the part of the scintillator detector in charge of processesing and analyzing (first analogically and then digitally) the electrical pulse given by the photosensor. The output of the electronic system is the useful information about the events detected such as number and energy spectrum.

In Figure 3.1 a scheme of a scintillation detector is shown. There, the scintillator detects ionizing radiation and produces photons that are guided by the reflector and the light guide to the photosensor. Some of the photons that reach the sensitive part of the photosensors are converted and multiplied, forming a electronic pulse. The output signal of the photosensor (electronic pulse) is processed and analyzed by the corresponding electronics:

¹The visible range is made up by photons with a wavelength between 380 nm and 750 nm

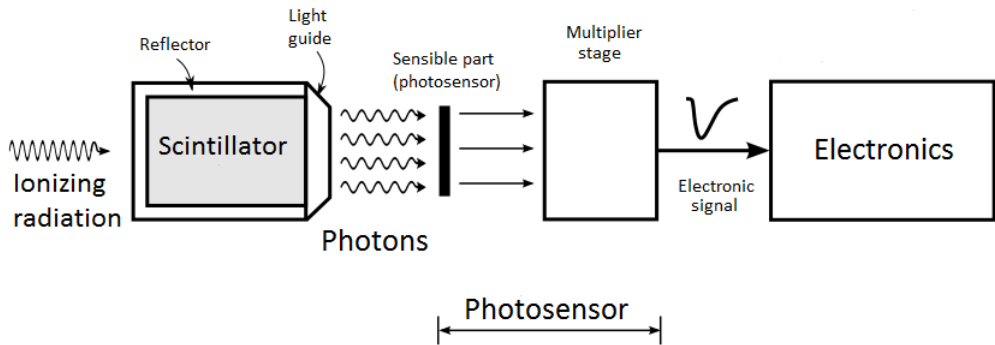


Figura 3.1 – Scheme of the scintillator detector

3.2.1 Interaction of Fast Electrons and Photons with Matter

This section describes the interaction of particles with matter, focusing on the particles and energy range relevant for this thesis, electrons (0–18 keV) and photons in the visible range (approx. 380 – 750 nm).

Electrons have charge so their interaction with matter is mainly with the orbital atomic electrons through the Coulomb force. The electron trajectory is much more tortuous than other heavier particles because the mass of both interacting particles is equal. Furthermore, for the same reason, these electrons lose a significant amount of energy in each collision. The specific energy loss is defined as $S = -\frac{dE}{dx}$ which gives the energy loss suffered by the particle per unit of path length. In the case of electrons, this total energy loss has two main contributions, the collisions (elastic and inelastic) and radiative processes (bremsstrahlung) [76, 77]:

$$\frac{dE}{dx} \approx \left(\frac{dE}{dx} \right)_c + \left(\frac{dE}{dx} \right)_{br} \quad (3.1)$$

The radiative part is roughly proportional to the collision part:

$$\frac{\left(\frac{dE}{dx}\right)_{br}}{\left(\frac{dE}{dx}\right)_c} \approx \frac{EZ}{700} \quad (3.2)$$

where E is the energy of the electron in MeV and Z is the atomic number of the absorbing material. Due to this energy loss, the electrons can only penetrate a material as far as they go before losing their total kinetic energy. This distance is known as range and, in the case of tritium electrons, its value is quoted in Table 1.4.

As photons don't have charge, their possible interactions with the matter are photoelectric effect, Compton effect, coherent scattering and pair production and the probability of each process depends on the energy of the photon, $E_\gamma = h\nu$, and on the atomic number of the material, Z , displayed in Figure 3.2.

The only relevant photons for this thesis are in the visible range, between 400 and 700 nm, that corresponds to energies of the order of the eV. Therefore, pair productions, which requires a photon energy equal or more than 1.022 MeV, does not play any role.

The photoelectric effect occurs when a photon interacts with an orbital electron in the material, losing all its energy. This energy is absorbed by the electron that is released from the atom (ionization). The energy of the resulting electron, E_e , is [76, 77]:

$$E_e = E_\gamma - E_b \quad (3.3)$$

where E_b is the binding energy of the electron in this material. The probability of this effect depends on the number of available electrons in the matter through the variable Z , and the energy of the electron according to

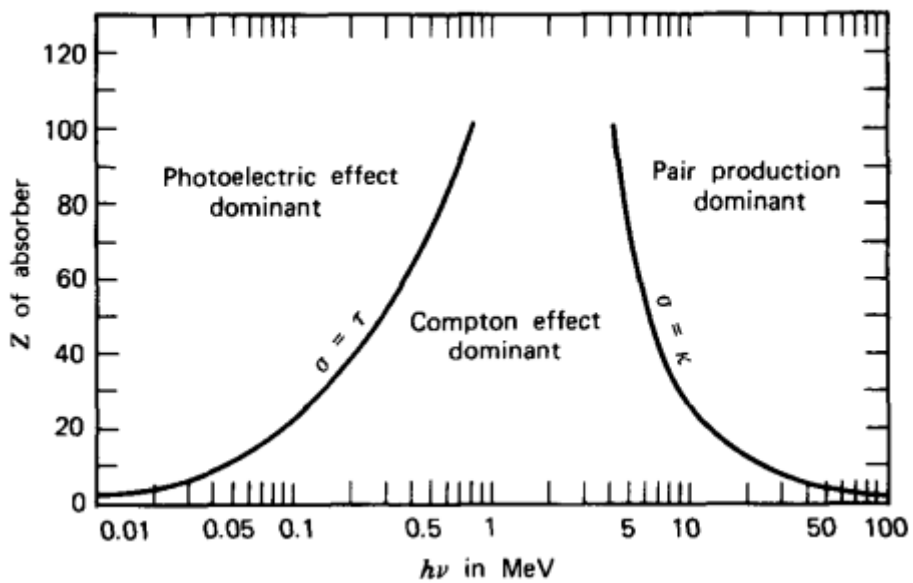


Figura 3.2 – Domain regions of the three most probable types of interactions of gamma rays with matter. The lines show the values of Z and $h\nu$ where the two neighboring effects are equally likely. [76, 77]

the expression [76]:

$$(Pr)_{Ph-eff} \approx \frac{Z^n}{E_\gamma^{3.5}} \quad (3.4)$$

Thus, the photoelectric effect is most probable for elements with high atomic number. This is the reason why elements with high atomic number are the best insulators against gamma radiation and why the passive shielding of TRITIUM monitor consists of lead bricks ($Z = 82$) (section 3.4.1).

The Compton effect occurs when a photon interacts with an orbital electron of the material, transferring part of its energy to the electron, which is released, scattered at an angle θ with respect to the original direction. If the electron binding energy is neglected, the energy, E_e transferred to it is given by [76, 77]:

$$E_e = \frac{\frac{E_\gamma^2}{m_0 c^2} (1 - \cos\theta)}{1 + \frac{E_\gamma^2}{m_0 c^2} (1 - \cos\theta)} \quad (3.5)$$

where m_0 is the rest mass of the electron and c is the speed of the light in the vacuum. The probability of the Compton effect is proportional to the atomic number (available electrons in the matter), Z , and decreases with the energy of the photon.

As can be seen in Figure 3.2, for photon energies in the visible spectrum (of the order of eV), the Compton effect is only likely for very light materials, ($Z < 4$). For heavier materials the photoelectric effect is the dominant effect.

Finally, for coherent scattering, the atom is neither excited nor ionized and the photon conserves all its energy in the collision. Coherent scattering is more probable for photons with low energies and materials with high atomic numbers and, as it will be shown in section 3.2.2, it explains

why the produced photons are guided along scintillating fibers.

3.2.2 Plastic Scintillators

Scintillators are widely employed for radiation detection in nuclear physics. Scintillator converts kinetic energy of the incoming particles in to light² which can be detected and quantified. Light emission happens through photon de-excitation of excited atoms.

Light production is linear in a wide energy range of incoming particles. Scintillators should have good optical properties, such as being transparent to the wavelenght of their own emission and having a refractive index as close as possible to that of glass for optimizing optical coupling with photosensors. Photon emission in scintillators is a stadistical process, which means that two identical events will emmit a different number of photons that follows a poisson statistics.

Scintillators can be organic and inorganic. Inorganic scintillators normally have a higher atomic number and density so their light output are higher. Due to these reasons they are better for gamma-ray spectroscopy. Organic scintillators are generally faster and they are commonly used for beta spectroscopy and neutron detection. This section is focussed on organic scintillators since they are the ones used in the TRITIUM project.

Organic scintillators are based on a scintillator material dissolved in a base solvent, normally aromatic hydrocarbons as C₁₈H₁₄, C₂₄H₂₂N₂O or C₁₅H₁₁NO with an average atomic numbers of which are between 3,5 and 5.

The scintillator molecules, in which the organic scintillators are based, have a π -electron structure. The energy levels of their electrons are

²The light is made up of photons in the visible energy range.

commonly illustrated with a Jablonsky diagram, shown in Figure 3.3, which shows the fundamental singlet state, S_{0i} , where the valence electrons are, the excited singlet states, S_{jk} , and the excited triplet states, T_{lm} . The energy difference between S_1 and S_0 states is around 3 or 4 eV, in the visible range. As it is shown in the figure, each energy states are splitted in close sublevels separated around 0.15 eV. This fine energy structure is due to excitations of molecular vibrational modes tabbed by the second index of the energy states. As the energy levels and sublevels have an energy larger than the thermal energy, 0.025 eV, non-excited electrons are in the ground state S_{00} at STP³.

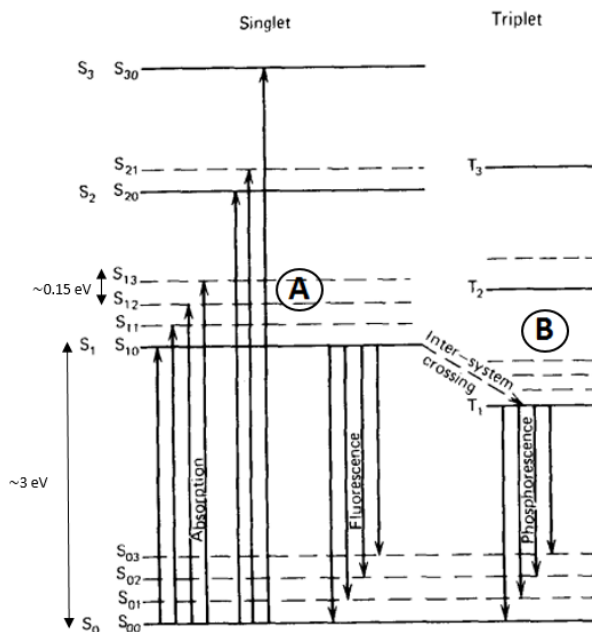


Figura 3.3 – Jablonsky diagram. [76]

When a particle deposits their kinetic energy in a scintillator, their valence electrons are exited to higher singlet energetic states very fast (times of the order of picoseconds) and are quickly de-excited to the first singlet

³Standar temperature and pressure conditions

excited state, S_{10} , through non-radiative processes known as internal conversion. These electrons can de-excited to the fundamental single state, S_{00} , through three different physical mechanisms:

- Prompt fluorescence (process A in Figure 3.3), where the electron in the S_{10} energy level is de-excited to some sublevel of the ground state S_{0i} , emitting a photon. This process happens immediately after the excitation of the scintillator molecules (around tens of nanoseconds after excitation). Each scintillator has a characteristic emission spectrum that defines its response due to the fluorescence mechanism.

Organic scintillators are practically transparent to their own fluorescence emission because there exist a quenching effect in each de-excitation process by which all emitted photons by the scintillator have less energy than the excitation. This effect is called Stokes shift and it is represented in Figure 3.4.

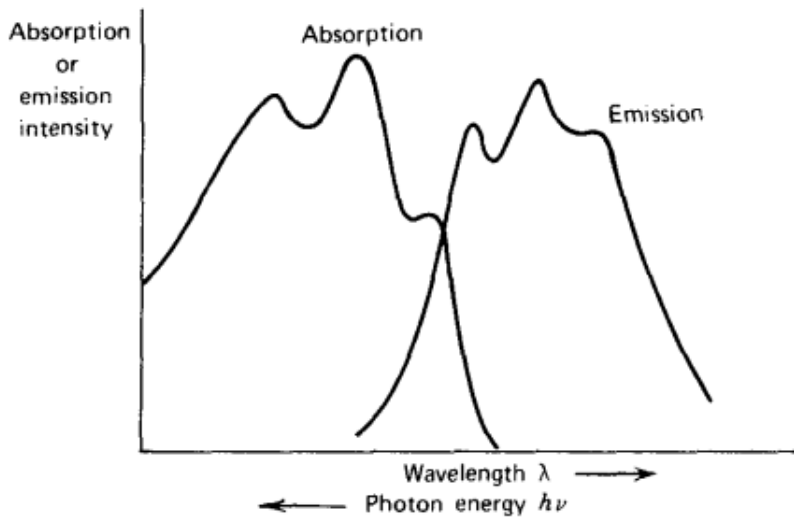


Figura 3.4 – Stokes shift. [76]

The intensity of the fluorescence emission in an organic scintillator over time is a combination of two exponential functions, one associated

with the lifetime of the level, τ (on the order of nanoseconds), and the other associated with the energetic level population, τ_1 (on the order of picoseconds) [76].

$$I = I_0 (e^{t/\tau} - e^{t/\tau_1}) \quad (3.6)$$

- Phosphorescence, where the electron that is in the first single excited state cross to a triple excited state (process B in Figure 3.3) with a process called "intersystem crossing". This is a metastable state with a longer lifetime than phosphorescence. This process happens around 10^{-3} seconds after scintillator excitation.
- Delayed fluorescence, which occurs when an electron is in a triple excited state but its transition to the ground state is forbidden. In this case, this electron interacts with another electron in a similar state, falling and return to the first singlet state and quickly de-exciting to the ground state.



This emission has the same emission spectrum as immediate fluorescence, but occurs later.

As the prompt fluorescence light produces the scintillator signal, detector design should increase it and reduce other possible physical mechanisms. One of the most important parameters is the scintillation yield⁴, defined as the the number of photons emitted by unit of absorbed energy. This yield depends on the type of particle and on other mechanisms that doesn't produce prompt fluorescence, like phosphorescence or delayed fluorescence

⁴The scintillation yield is a way of expressing the efficiency of the scintillator in converting the energy deposited by the particle into photons.

or even internal conversion. The scintillator yield is normally quoted by the manufacturer for mips⁵.

Plastic scintillators are easy to machine to any desired shape. The chosen shape for TRITIUM detector is the fiber, specifically, commercial fibers BCF-12 from Saint-Gobain Crystals Inc company [78]. This type of fiber was chosen as the result of a comparative study [79] among some of the best-known commercial manufacturers.

The BCF-12 fibers consist of a scintillating of polystyrene with the possibility of surrounding it by a cladding of polymethylmethacrylate (PMMA) (smaller refractive index than core in order to achieve a critical angle) or a multicladding (second cladding) with even smaller refractive index.

When a particle deposits all or part of its kinetic energy, some photons are produced in the fiber core as a result of the scintillating process. The number of photons produced depend on the scintillation efficiency and its value is around 2.4% for the fibers used (BCF-12), which means that a scintillation yield of 8000 photons will be produced per MeV for a mip. For instance, for tritium electron, these fibers release a maximum of around 148 photons (when tritium electron has the maximum energy, 18.6 keV), or less as electrons of these energies are not mips. The emission spectrum of the fibers employed in this work, is shown in Figure 3.5.

The scintillation light is guided to the sensitive part of the photosensor. A single photon produces a signal with some probability, called the quantum efficiency. Fibers (and scintillators in general) use the optical property of Snell's law [80] to guide their photons to the desired part (ends of the fibers). It is based on the interface created between the core and the surrounding material. When a photon hits this interface, it is refracted

⁵The MIP, Minimum Ionized Particles, is a particle that has the speed that generate minimum ionization, that's, for example, electrons with 500 keV or more

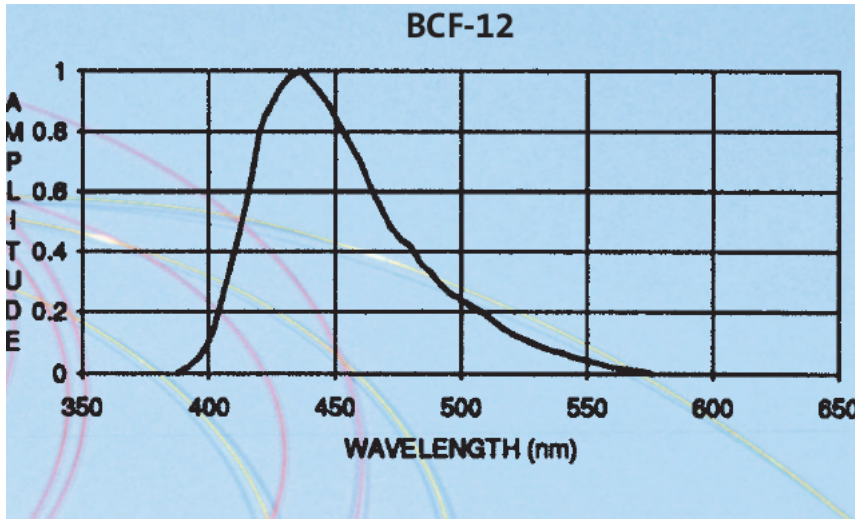


Figura 3.5 – Emission spectrum of BCF-12 fibers of Saint-Gobain. [78]

(and therefore lost) following the Snell equation, 3.8 [80].

$$n_0 \sin(\theta_0) = n_1 \sin(\theta_1) \longrightarrow \theta_c = \arcsin\left(\frac{n_1}{n_0}\right) \quad (3.8)$$

If the surrounding material has a lower refractive index than the core of the fiber, there exist a critical angle, θ_c , beyond which photons will be totally reflected and therefore kept within the fiber as illustrated in Figure 3.6.

The trapping efficiency or photon collection efficiency is defined as the efficiency of the scintillator to guide photons. For BCF-12 fibers with optical clad is between 3.44% and 7% per meter of fiber (depending on where the event is detected and is minimum near the fiber axis and maximum near the core-clad interface. For no clad fibers BCF-12 surrounded by water, the trapping efficiency is larger than for cladded fibers. Therefore, from the maximum of 148 photons initially created by a tritium decay electron with the maximum energy, only 41 photons (for maximum trapping efficiency)

are guided in the 25 cm fiber length used in the TRITIUM detector. Thus, the output signal is very weak and is in the range of the spectrum where electronic noise is already significant. As described in the following chapters, a great effort was made to minimize electronic noise by different techniques.

In Figure 3.6 the light collection in a fiber is illustrated.

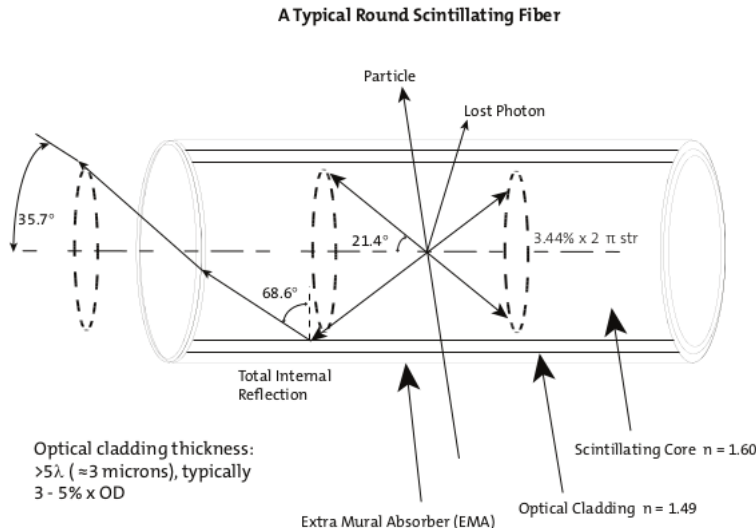


Figura 3.6 – How photons are collected in a fiber with single clad. [78]

The cladding material is useful for protecting the core surface from dirt or aggressive external agents that may reduce the light collection but at the cost of increasing the critical angle which its corresponding loss of light. Three different cases are shown in Table 3.1, where the cladding effect is illustrated.

In the practice, it is difficult to achieve a perfect air-core or water-core interface which affects light collection. As commercial claddings are thicker (30 μm) than the mean free path of tritium decay electrons in water (around 5 μm) cladded fibers is not an option for the TRITIUM detector. Hence, special attention is needed for achieving a water-core interface good enough. To overcome this problem a special protocol was developed in the

Material	Refractive index	critical angle ($^{\circ}$)
Air	1	42.98
Water	1.33	62.47
Cladding of PMMA	1.49	76.26

Table 3.1: Critical angles associated to different interfaces created with polystyrene, $n_0 = 1.6$, and other materials

ICMOL laboratory for preparing fibers for tritium detection.

The most important parameters of scintillating fibers of TRITIUM are given in Table 3.2.

3.2.3 Light Detection in Photosensors

The scintillating photons created in the core of the fiber and guided to its end are detected by photosensors. Photosensors have a sensitive part that is optimized to detect photons in a range of energy (usually in the visible range) with a certain probability, called quantum efficiency. The photosensors produce an electronic signal that carries information about the detected photons such as number and detection time.

There are many available photosensors that rely on various physical processes, such as photoelectron multiplier tubes (PMTs), silicon photo-electron multiplier (SiPM) or charge-coupled device (CCD).

To optimize the efficiency of a scintillation detector is essential that the emission spectrum of the scintillator (Figure 3.5 for the fibers used) overlaps as much as possible with the detection efficiency spectrum of the photosensor chosen. The detection efficiency spectrum shows the probability of detecting photons at a function of wavelength. The efficiency of a detector is proportional to the product of both the emission and the

Core material	Polystyrene
Core refractive index	1.60
Density (g/cm ³)	1.05
Cladding material	Acrylic (PMMA)
Cladding refractive index	1.49
Cladding thickness (μm)	30
Numerical aperture	0.58
Trapping efficiency	3.44% minimum
No. of H atoms per cc (core)	$4.82 \cdot 10^{22}$
No. of C atoms per cc (core)	$4.85 \cdot 10^{22}$
No. of electrons per cc (core)	$3.4 \cdot 10^{23}$
Radiation length (cm)	42
Emission peak (nm)	435 (Blue)
Decay Time, (ns)	3.2
1/e Length (m)	2.7
Scintillator yield (# γ /MeV)	~ 8000
Operating Temperature	-20°C to 50°C

Table 3.2: Properties of BCF-12 fibers from Saint-Gobain Inc. [78]

detection efficiency spectra and this is largest when both spectra match.

The proposal of TRITIUM is to use SiPM arrays because they are very fast (of the order of ns) and have a high photodetection efficiency of about 50%, high gains (multiplication factor of 10^6) and a low voltage supply. The most important reason of this choice is that SiPM arrays are able to detect a single photon with high efficiency, which is a fundamental aspect due to the low amount of photons generated by tritium decay. The PMTs, which are the conventional choice, were also tested because they have lower dark count rate than SiPM and similar properties like gain and timing.

Photoelectron Multiplier Tubes (PMTs)

Photoelectron multiplier tube, PMT, employed as photosensors in nuclear physics during decades, detect the scintillating photons that reach its sensitive part, photocathode, and produce an electronic signal, large enough to be easily measured. In Figure 3.7 a schematic drawing of a PMT is given. The PMT consists of a vacuum tube that has a glass window through which photons can penetrate. The electrons created in the photocathode travel in vacuum.

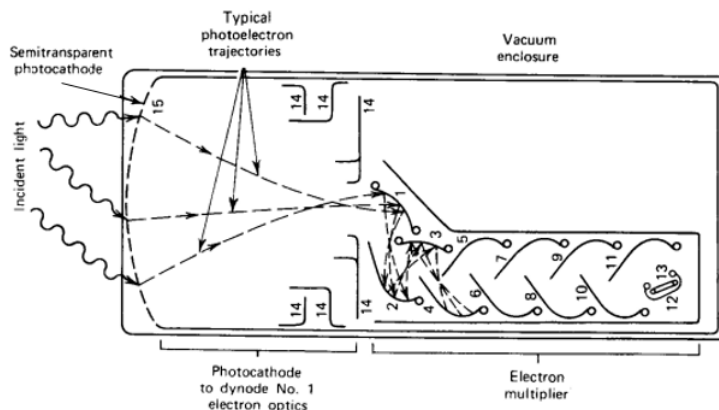


Figura 3.7 – Scheme of a PMT. [76]

The signal production has two phases:

1. In the photoathode photons are converted in photoelectrons through photoelectric effect. The photocathode consists of a thin layer, of the order of nanometers, deposited on the inner surface of the PMT window. The material of the photocathode is chosen to optimize the probability of producing photoelectric effect with the scintillating photons. The PMTs used in TRITIUM experiment are the model R8520-406 from Hammatsu [81] and the material of their photocathode is Bialkali⁶.

⁶The bialkali material is based on the elements ^{121}Sb , ^{85}Rb and ^{132}Cs

The response of the PMT at long wavelengths is limited mainly because photon energy is not enough to produce a photoelectric effect or the emitted photoelectron does not have enough energy to overcome the material-work function. The response of the PMT at short wavelengths is limited due to absorption in the window material, quartz in our case. Thus, the response of the PMT has a strong dependence on the energy of the photon and the quantum efficiency (QE) spectrum defined is given by the ratio of the number of photoelectrons produced at the cathode of the PMT and the number of photons reaching it. For PMTs used in the TRITIUM experiment, the QE is showed in Figure 3.8.

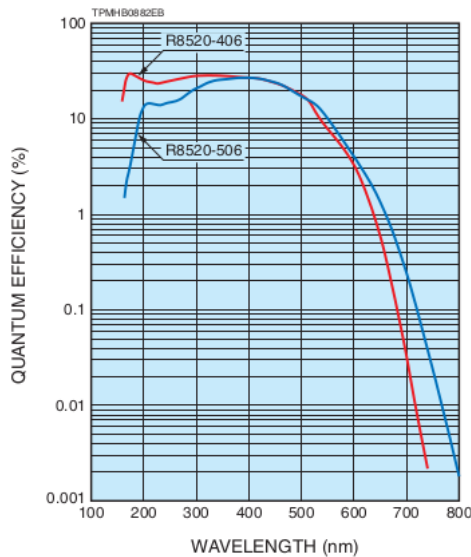


Figura 3.8 – Quantum efficiency spectrum for the PMT used (R8520-406). [81]

The maximum values of the PMT quantum efficiency is usually between 20% and 30% [76] (a little bit less than 30% for the PMTs employed). The emission spectrum of the scintillating fibers used, Figure 3.5, matches the quantum efficiency spectrum of the PMTs used, Figure 3.8 and the position of both peaks is very close, 435 nm

for fibers and 420 nm for PMT.

2. As the number of photoelectrons produced in the photocathode is very small, an electron multiplication stage is employed to obtain an electronic signal of sufficient size to be processed by the electronic system. The amplification stage is based on three elements, focusing electrodes, dynodes and anode, which are metallic plates with a shape and position designed to optimize the collection and multiplication of electrons. A high voltage (HV) is applied to the PMT which is distributed between all this elements, including the photocathode, with the help of electronic circuit. A positive HV, grounded in the photocathode, is interesting for measuring PMT currents, and a negative HV, grounded in the anode, gives a faster response. The commercial electronic circuits of Hammatsu are shown in Figure 3.9.

Focusing electrodes guide the photoelectrons to the first dynode. They have an collection efficiency (CE) defined as the ratio of the number of photoelectrons reaching the first dynode and the number of photoelectrons leaving the photocathode and its value is around 80%. The dynodes achieve the electron multiplication. A voltage difference between adjacent dynodes accelerates the electrons and produce their multiplication. The multiplication factor of each dynode, δ , is commonly around 5 and is strongly dependent on the HV. If all dynodes have the same gain, the overall gain of a PMT with N dynodes is [76]:

$$G = CE \cdot \delta^N \quad (3.9)$$

that give an overall gain of a PMT of the order of 10^6 , strongly dependent on the applied HV.

The multiplication stage adds an uncertainty in the measurement. Working without gain allows to count the number of photons that reach the PMT. This can be done by short-circuiting all the dynodes and the anode and collecting the signal directly of the photocathode. This special setup was used for fiber characterization, described in

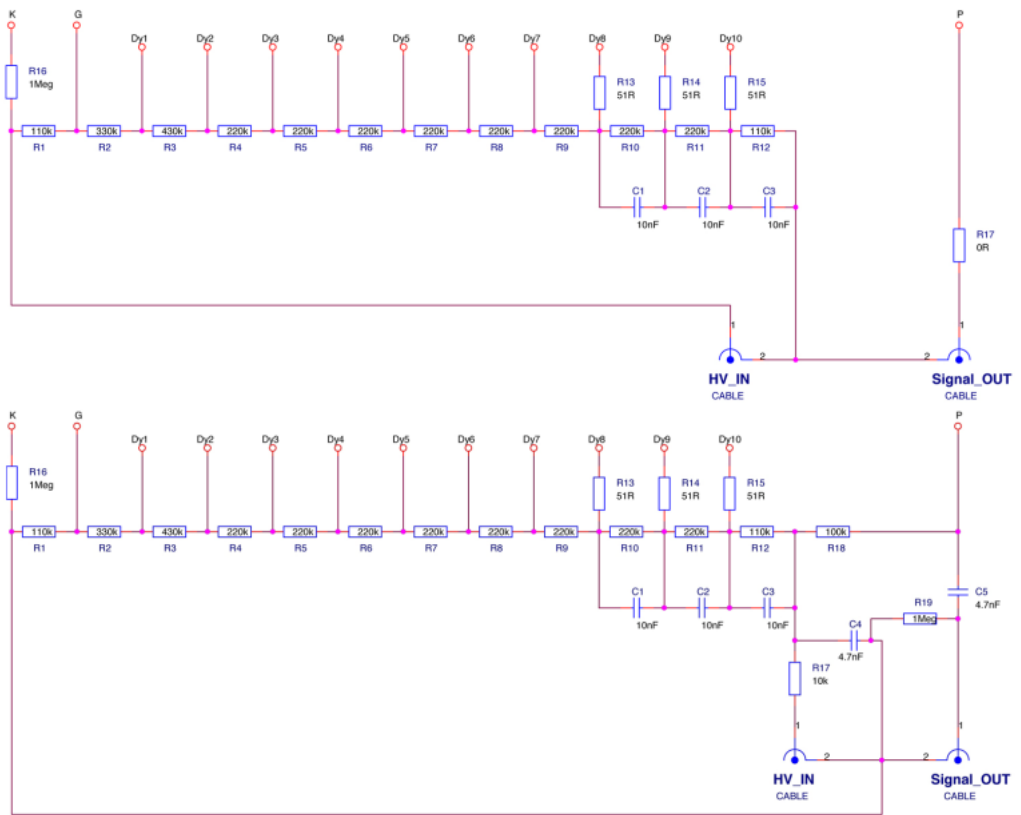


Figura 3.9 – Hamamatsu commercial voltage divider electronic circuit. Upper circuit with negative supply and lower circuit with positive supply. [81]

section 4.1.3.

The output pulse of a PMT has a width of the order of tens of nanoseconds. The multiplication process can be described as a Poisson statistical process. For each electron in the first dynode, G new electrons are created with a variance of \sqrt{G} .

The output signal of a PMT is linear with the number of photons that reach its sensitive part up to a saturation limit, at which the linearity is lost. This limit depends on the PMT model.

The photocathode may emit electrons without any scintillation light. This signal is named dark current, I_{DC} , and can arise due thermoionic emission and, for the PMTs used, this value is around 2 nA according to their data sheet.

The characterization of the PMTs used for dark current, gain for several HV and quantum efficiency, was done at IFIC in the framework of NEXT experiment [82].

Silicon Photoelectron Multiplier Array (SiPMs array)

The Silicon Photomultiplier (SiPM) are a bind of photosensor, based on semiconductor materials, developed in recent years. They are replacing progressively conventional PMTs in many experiments and applications. They achieve outstanding photon-counting capabilities with high gain and high photodetection efficiency comparing to PMT. They have convenient characteristics as insensitiveness to magnetic fields, low operating voltage and compactness.

SiPM are based on p-n junctions, made with special techniques to achieve a good contact between both surfaces.

The voltage at which the SiPM changes from proportional to geiger mode is called the breakdown voltage, V_{BR} . At a lower voltage it works in proportional mode but at a higher voltage, it switch to Geiger mode. The measurement of the breakdown voltage is one of the most important parametes to characterize the SiPM and Its determinations is described in section 4.2.

The SiPM, formed by a matrix of APDs which are photodiodes operating in Geiger mode. A scheme of an APD is shown in Figure 3.10. It has p+ and a n+ layers.

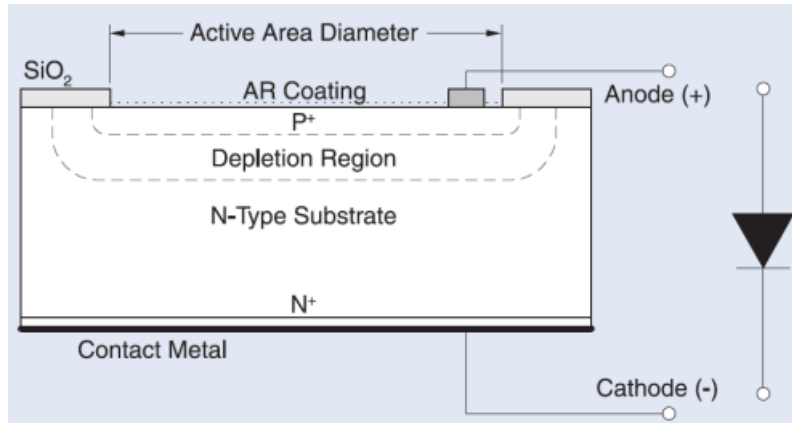


Figura 3.10 – Scheme of a APD and electrical symbol used. [84]

These APDs, called pixels when they are part of a SiPM, are connected in parallel and the sum of all of them is read. The output signal of the pixels are quite similar regardless of the energy deposited, with some difference because of the uncertainty due to the SiPM manufacturing process and the statistical nature of the detection process. The energy deposited in each APD is not known but, as all SiPM pixels are read at the same time, the charge of the output signal when n photons are simultaneously detected is n times the charge of a single photon, as can be seen in Figure 3.11. Due to this property, after a correct calibration of SiPMs the number of detected photons we have detected is linearly related to the output signal.

As the number of scintillating photons is proportional to the deposited energy, the linearity of its output signal and the deposited energy is obtained.

On top of that, these pixels need to be so small⁷ that, if the photon density to be detected is low enough, we only detect one photon in each pixel. If it doesn't happen, we will detect two or more photons with the same pixel but the output signal will be the same as one detected photon, so

⁷Pixel sizes for commercial SiPMs are 50 or 75 μm [85], [86]

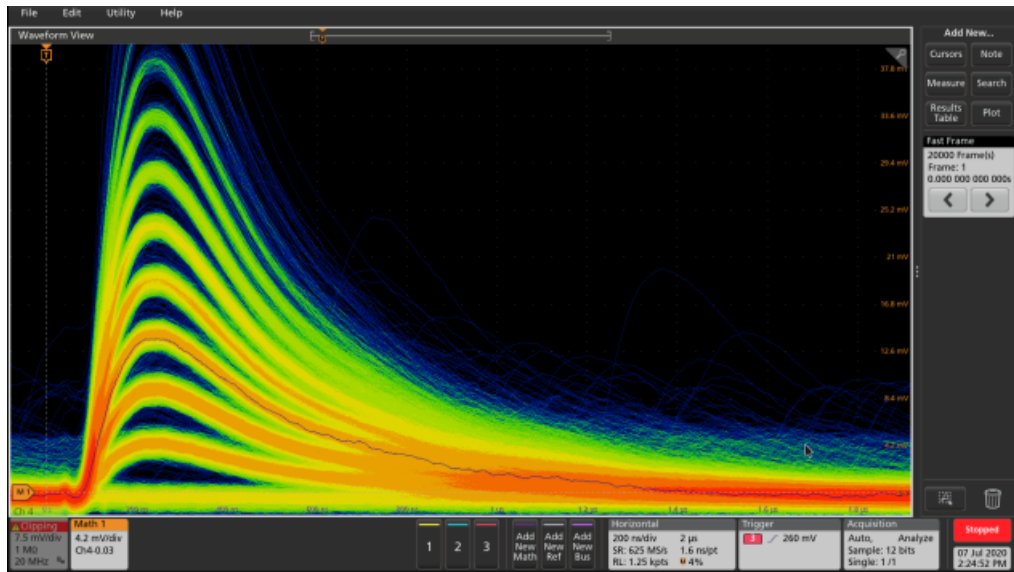
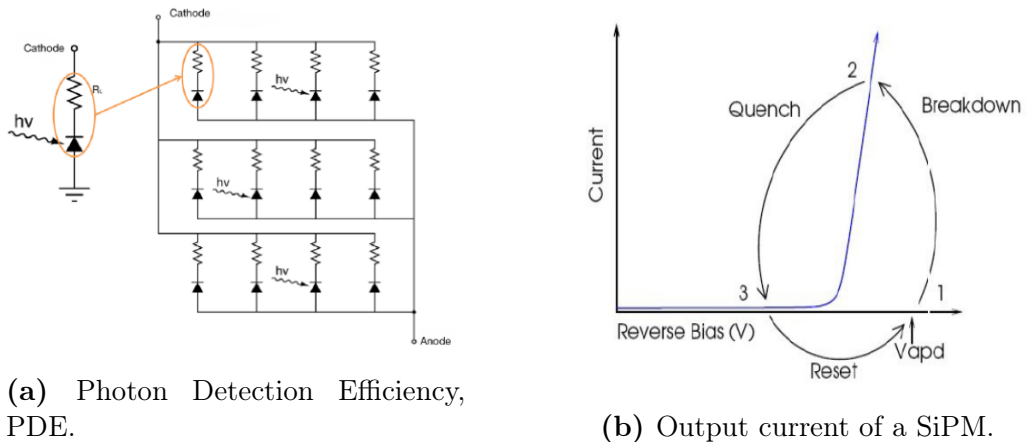


Figura 3.11 – Using persistence on the oscilloscope to show several pulses with different heights. Each height associated with a different number of SiPM pixels lit at the same time.

we will have a loss of linearity of our output signal. This effect is known as saturation and it is important to know the photon density at which it happens for our SiPMs. The experimental measurements of this effect, which have been done for our SiPMs, is shown in section 4.2. SI LA MIDO YO PERFECTO, SI NO DECIR QUE PARA NEUSTRO CASO NO ES IMPORTANTE PORQUEU ESTAMOS MIDIENDO MUY POCOS FOTONES POR EVENTO.

Each of these pixels has a quenching resistance⁸ in series that is used to stop the current produced when this pixel has detected a particle. It is used for limit the current drawn by the diode during breakdown and reduce the reverse voltage seen by the diode to one below the breakdown voltage. After that, the voltage seen by the diode is reset to the bias voltage and this pixel is ready to detect a new particle again. In Figure 3.12 (left)

⁸The tipical valuer of this quenching resistance for commercial SiPMs is around 500 kΩ



(a) Photon Detection Efficiency, PDE.

(b) Output current of a SiPM.

Figura 3.12 – (Left) Electronic scheme of a SiPM and (right) output current of a SiPM as a function of the reverse voltage. It show that the quenching mechanism is essential for working with SiPMs [89].

a diagram of these chenching resistances and APDs in a SiPM and (right) how it works is shown respectively.

In this simple electrical scheme we can see that all pixels have a common cathode and anode which means that, as we said before, they are at the same bias voltage and the output is the sum of all of them.

We have a lot of names to refer to these photosensors such as SiPMs, MPPCs, G-APDs, SSPMs, MRS-ADPs or AMPDs. The candidate for TRITIUM project is S13360-6075 from Hamamatsu photonics [86] because its characteristics are the ones that best fit our objectives since this model has super low afterpulses, crosstalk and dark counts than other SiPM models from Hamamatsu. Its characteristics and properties are shown in Table 3.3.

These values, provided by Hamamatsu photonics, are only approximate for a given element so. Therefore, these parameters must be determined experimentally for each SiPM because they can vary significatively

Parameter	Numerical value
Serie	S13360
Model	6075
Pixel Pitch (μm)	75
Effective photosensitive area (mm^2)	6.0×6.0
Number of pixels	6400
Fill factor	82%
Refractive index of windows material	1.55
Operating temperature range ($^\circ\text{C}$)	[−20, 60]
Spectral response range, λ (nm)	[320, 900]
Peak sensitivity wavelength, λ_p (nm)	450
PhotoDetection Efficiency, PDE, $\lambda = \lambda_p$ (%)	50
Dark counts, Typical/Maximum (kcps)	2000/6000
Terminal capacitance, C_t (pF)	1280
Gain, M,	$4 \cdot 10^6$
Breakdown Voltage, V_{BR} (V)	53
Cross talk probability(%)	7
Temperature coefficient ΔTV_{op} ($\text{mV}/^\circ\text{C}$)	54

Table 3.3: Characteristics of SiPM S13360-6075 from Hamamatsu Photonics [86].

even for SiPMs of the same model. The most important characteristics for the TRITIUM project are experimentaly measured and given in section 4.2.

Although TRITIUM detector uses whole SiPM matrices, the characterizations has been carried out at the level of a single SiPM (same model) to learn the values of the SiPM parameters and to test the gain control method.

The matrices selected are of the model "S13361-6050" from Hamamatsu, which consists of a 4×4 SiPM matrix where the active area of each SiPM is 6×6 mm [87] or the model "S13361-3050" from Hamamatsu, which consists of a 8×8 SiPM where the active area is 3×3 mm [88]. They are commercial matrices from Hamamatsu and the total active area that they cover is the same for both models, 24×24 mm and it is approximately the same as the active area covered with the PMTs employed, described in the previous section. These matrices have a common bias voltage and ground for all SiPMs but a different output signal for each SiPM.

Comparison of photosensors considered

The photosensors employed in TRITIUM are both, PMT and SiPM. Each kind of photosensor has his advantages and disadvantages, so both were tested to make a final choice. The output signal of both photosensors is proportional to the number of incident photons and they have a similar gain (of the order of 10^6). Both properties are essential to detect tritium events and to obtain a signal large enough to be measured and processed. Both photosensors have fast output signals, with a rise time shorter than nanoseconds, and a wide spectral sensitivity (200 – 800 ns for PMT and 300 – 900 ns for SiPM). The supply voltage necessary to work with SiPM, on the order of tens of volts, is much lower than that of PMTs, which require a high voltage, of the order of a thousand volts. The PDE at 420 nm, achieved with SiPM is higher, around 50%, than with PMT, which have a PDE about

30%. A large PDE is essential because the number of photons produced in a tritium event is very low. Furthermore PMTs, as they consist of a vacuum tube, are more bulky and fragile than SiPMs, which are compact and robust. This is an advantage for the SiPMs because TRITIUM detector should work during years. Furthermore, PMTs are rather more expensive, than SiPMs. In addition, PMTs are affected by magnetic fields, contrary to SiPMs that works correctly in intensities of magnetic field up to 7 Tesla. Moreover, due to their high uniformity, SiPMs are capable of distinguishing the exact number of photoelectrons detected and even of resolving a single photoelectron, which is not possible with PMTs due to variations in their gain.

On the other hand, the dark current of PMTs is much lower (a few counts per second) than that of SiPMs, that have a dark current between 0.1 and 1 Mcps⁹, depending on their size, and this happens almost entirely at the level of a single photoelectron. This prevents to separate tritium decay signals from background in the signal photon-detection zone. Another inconvenient of SiPMs is large crosstalk and afterpulses that need to be corrected.

An additional drawback of SiPMs is that their output signal depends strongly with the temperature. As TRITIUM detector will be installed in an environment with significant temperature variations, this problem is solved by a suitably changing the supply voltage to compensate temperature variations.

3.2.4 Electronic Readout

The electronic system is in charge of reading, processing and analyzing the output signal of photosensors and providing output information about the

⁹Mega counts per second, 10^6 c/s

tritium detection. This electronic system depends on the type of detector configurations employed

Electronical system for PMTs

PMTs were used in TRITIUM experiment for two main objectives. On the one hand, to know the amount of incident photons that reached the PMT photocathode, which is important to characterize fibers, and, on the other hand, to know the energy of events, which allow us to obtain an energy spectrum and to discriminate events according to their origin.

To know the amount of photons that have reached the photocathode, the PMT should work without internal gain since it introduces a large uncertainty in the measurement. To this end, the electron multiplication stage (shown in section 3.2.3) must be bypassed. This is achieved with the help of a PCB, shown in Figure 3.13, designed, built and tested for this purpose.

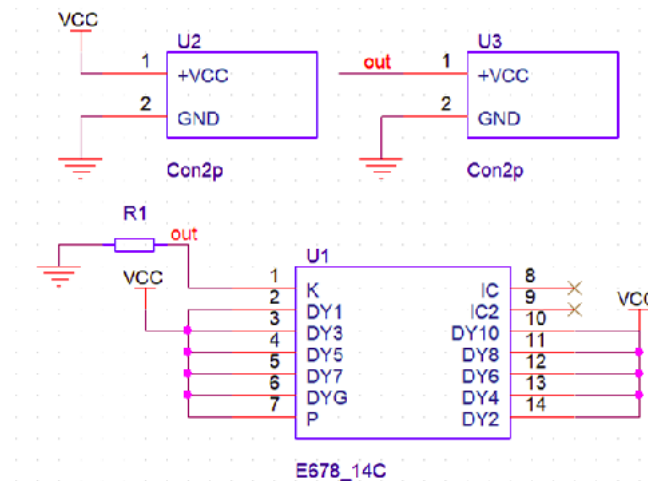


Figura 3.13 – Electronic scheme of the electronic voltage divider circuit used for working with PMTs without its internal gain.).

This PCB short-circuit the dynodes and reads the signal directly from the photocathode. This PCB was designed to be supplied with a positive voltage smaller than usual running voltage because It is only needed to create a voltage difference between the photocathode and the first dynode. As the signal is not multiplied, the output pulse of the photosensor is very small (currents of the order of tens of nanoamperes and a special readout system is needed. The chosen system is Keithley 6487 Picoammeter/Voltage Source [90], a commercial system from Keithley. This system has some useful options such as automatic baseline correction, the ability to read currents of the order of picoamperes and the possibility of carrying out mathematical operation on the signal, such as the average of N measurements with the associated statistical error, where N is programmable by the user ($N = 100$ in all our studies). This is the configuration set to measure the output current of our photosensors. The number of photons that has reach the photocathode is calculated from:

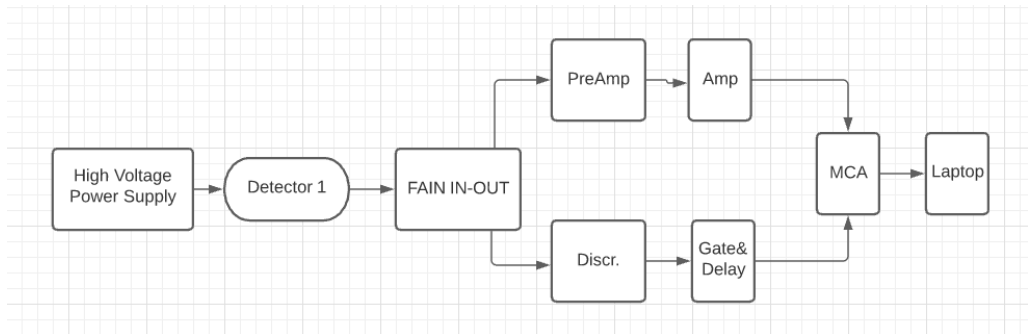
$$N^o \gamma / \text{sec} = \frac{(I_{PMT} - I_{DC})}{q_e \cdot QE \cdot CE} \quad (3.10)$$

where I_{PMT} is the output current of the PMT when it detects photons and I_{DC} is the dark current. This equation takes into account the quantum efficiency of the PMT, which is close to 30%, and the capture efficiency in the dynodes, equal to 1. In addition, it is assumed that each detected photon only generates one electron, the charge of which is q_e .

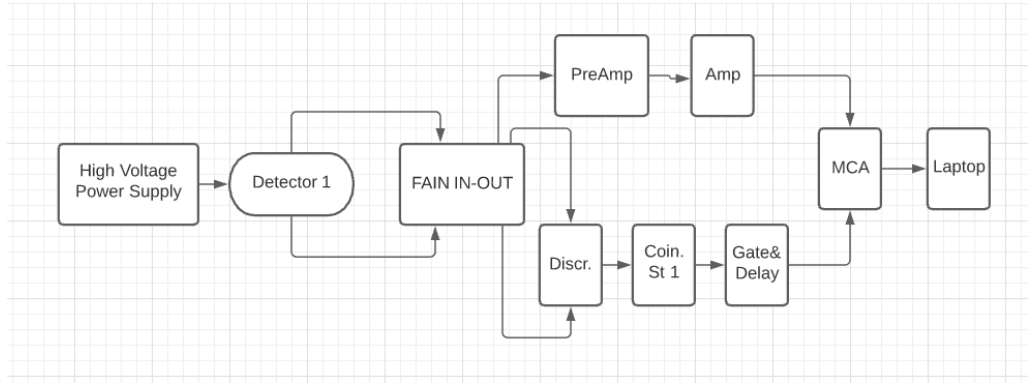
To determine the energy of the events, the internal gain of the PMT has to be restablished.

The number of PMTs used are one, two or four, depending on the measurement. A simplified scheme of the electronic chain employed in each case is shown in Figures 3.14a, 3.14b and 3.14c, based on various NIM technology modules¹⁰.

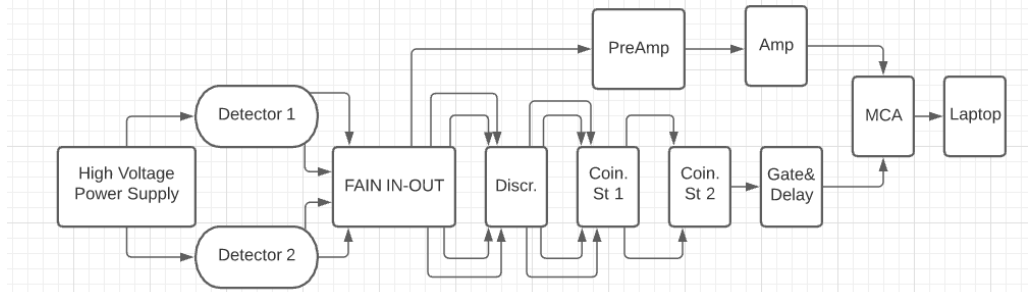
¹⁰The Nuclear Instrumentation Module (NIM) is a standard specification convention for electrical and mechanical parameters defined in electronic modules used in experi-



(a) Electronic scheme employed when only one PMTs are used in time coincidence.



(b) Electronic scheme employed when two PMTs are used in time coincidence.



(c) Electronic scheme employed when four PMTs are used in time coincidence.

Figura 3.14 – Schemes of the different electronic for measuring with PMTs.

The PMTs are supplied in all the cases by TC 952 High Voltage Supply from Tennelec [91], which has four channels. If two or more configurations are needed, a second voltage supply HV Power Supply N 1130-4 from Wenzel Elektronik company [92] with 4 additional channels, was employed.

As it can be seen in the figures, there are two different lines followed by the PMT output signals, the amplification line and the time coincidence line. Therefore, the first module needed is an analogic FAN IN-OUT module which is used to duplicate the input signal. The module employed is the Quad linear FAN IN-OUT MODEL 740 from Philips Scintific [93], which has four channels. One output signals is used as the input for the amplification part and a second is used as the input for the time coincidence part.

1. The amplification line, which is the same for the three configurations, provides the energy information and is based on two steps:
 - (a) One of the output signals is integrated by a preamplifier, which gives an output signal with a height corresponding to the charge of the input pulse. This signal has a long tail¹¹ produced by the preamplifier capacitance. The preamplifier used is "MODEL 9326 FAST PREAMP" from ORTEC [94].
 - (b) The output signal from the preamplifier is lead to the amplifier which gives an amplified output with a shape close to a Gaussian function. The used amplifier modules are 575A and 671 from ORTEC [95, 96]. An example of the output signal for 575A module is shown in Figure 3.16, green color.
2. The time coincidence line contains the time information and gives the gate that triggers coincident signals of both PMTs. This line consists of:

mental nuclear and particle physics.

¹¹The length of the tail is, $\tau = RC$, where R is the input resistance and C is the capacitance used. It is the typical output signal in RC circuits.

- (a) One of the output signals of the FAN IN-OUT module of each PMT is introduced into a discriminator module that gives a logic signal of -1.2 V height and of 240 ns width when a given threshold is exceeded. The discriminators utilized are Octuple Constant-Fraction Discriminator CF8000 module from ORTEC [97] and 4 channels discriminator model 84 from CAEN [98].
- (b) Time coincidences are required to ensure that detected event comes from the scintillating fibers and to remove background like external light and dark current.

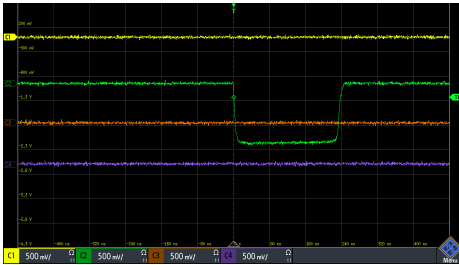
The two logic signals given by the discriminator module that come from the two PMTs in the same detector are introduced in the coincidence module which generates an output signal of -1.4 V height and of 20 ns width, when both are in coincidence. The modules used are Coincidence Unit Model 465 from LeCroy [99] and Coincidence Type N6234 from CERN-NP [100].

- (c) Time coincidence of two different detectors (4 PMTs, configuration 3.14c was also studied, which is useful to remove background due to hard cosmic radiation.

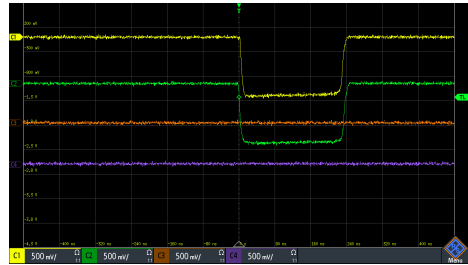
To do so, a new coincidence step similar to the previous one must be applied. The two logical output signals of the single detector coincidence are checked for coincidence.

Some examples are shown in Figure 3.15 for time coincidences of two detectors (4 PMTs). There, four logical signals are shown, two of them (channel one and two, yellow and green respectively) come from two PMTs connected to the first detector and the other two signals (channels three and four, color orange and violet respectively) come from PMTs connected to the second detector.

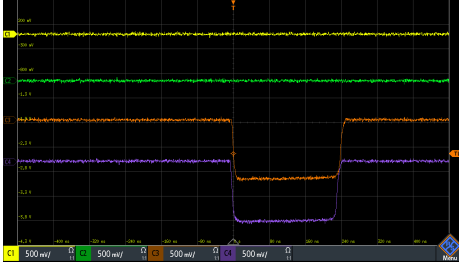
- i. In Figure 3.15a only one PMT (channel two) has detected an event. It means that the event is likely not produced in the scintillator. In this case, no output is generated.
- ii. In Figures 3.15b and 3.15c two PMT signals of the same



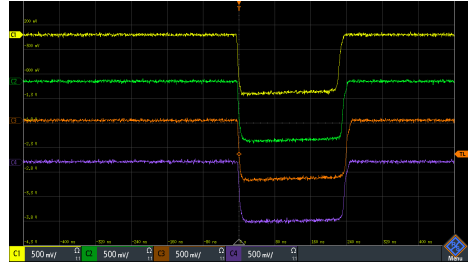
(a) Event detected in only one PMT, one detector.



(b) Event detected in two PMTs, one detector.



(c) Event detected in two PMTs, other detector.



(d) Event detected in all PMTs, both detector.

Figura 3.15 – Different situation that can happen when time coincidences with PMTs are done.

detector are generated but the other detector gives no signal. This event is discarded.

- iii. In Figure 3.15d the four signals are detected, which means that the output signal is generated and the event is recorded.
- iv. The logical output signal, is introduced in the Gate and Delay Generator, model 416A of the company ORTEC [101], which gives a positive logical signal, shown in Figure 3.16, orange color, with a height of 8 V and width of 2 μ s.

At the end, a logical and analogical signals are obtained, shown in Figure 3.16, which are recorded by the MCA 8000D, Pocket MCA from AMPTEK [102]. The analogical signal has information about the energy of the event and this is the signal whose information we will save for analyz-

ing. On the other hand the logic signal (output from the Gate and Delay Generator module) that indicates when the amplified signal must be saved.



Figura 3.16 – Signal amplified and logical gate (input signals of MCA).

The MCA is a module used to record the signal height as a histogram. The height of the signal (green signal) corresponds to the energy of the event and, when there is a gate (orange signal), is recorded.

Electronical system for SiPMs

The SiPMs are used in the TRITIUM experiment in two different ways, at the level of a single SiPM and at the level of several SiPMs arranged in a matrix. Both studies were carried out to characterize the SiPM arrays used in the TRITIUM monitor.

The electronic system chosen to process and analyze the output signals of the SiPM arrays is PETsys [103], which is a commercial system prepared to work with SiPM matrices from Hamamatsu.

PETsys is a complete acquisition and digitization system that is capable of working with up to 1024 SiPM. This system consists of a basic board, which processes the signal, to which 16 different SiPM matrices can be connected with up to 64 SiPM per matrix. This number of channels is needed in the TRITIUM project because, as it is shown in section 5.3, the TRITIUM monitor consists of a large number of SiPM matrices with 16 channels (SiPMs) per matrix. The PETsys system used in TRITIUM is displayed in Figure 3.17.



Figura 3.17 – Different parts of PETSYS system. [103]

Although the capacity provided by PETSYS should be enough for the requirements of the TRITIUM project, TRITIUM is a modular detector with scalable sensitivity. It means that, if an improvement of its limits is needed to improve its sensitivity or to further reduce the background, more photosensors would be needed. Therefore, the electronic system should be able to increase its capacity in a scalable way. This requirement is fulfilled by PETSYS since it has an additional module, called Clock and Trigger, to which up to sixteen different PETSYS basic boards can be connected. These sixteen PETsys basic boards are read in parallel, giving a total system

capacity of reading 256 SiPM matrices (16384 SiPMs¹²).

PETSYS is based on C++ and Python scripts that are prepared for the main tasks required, such as time coincidence options between SiPM (or even SiPM matrices) or energy discrimination. It is open source, giving the possibility to modify the current scripts or develop others with additional functions. PETsys has a time resolution of 250 ps which is one of the best time resolutions of commercial systems available and its price is around 10€/ channel, which is cheaper compared to similar electronic systems.

As described in section 4.2, the SiPM matrix temperature is an important parameter. The PETsys system has the ability to monitor the temperature of the SiPM matrices and ASICS employed to control them. Temperature monitoring is important to ensure the correct functioning of both, photosensors and system. PETsys has the possibility of developing new function scripts to implement the stability gain method reported in section 4.2.

Although the TRITIUM monitor use SiPM matrices it is important to start the characterizaton at the level of a single channel (only one SiPM) to reduce the uncertainties in the first results. In order to do so, an electronic system was designed, developed and built to read up to eight different SiPMs and to monitor their temperature.

This system is based on three different PCBs¹³, shown in Figure 3.18 (electronical schemes shown in the appendix A):

1. The first PCB, shown in Figure 3.18a, is used to organize the SiPMs and sensor temperature. This PCB place up to 8 different SiPMs and a temperature sensor and arrange their output signals on two HDMI connections. This PCB is placed inside a special black box, from

¹² $1024 \cdot 16 = 16384$

¹³PCB, Printed Circuit Board

Thorlabs company [104], that has a high degree of light tightness. This black box has a small hole of 1 mm diameter, prepared to introduce an optical fiber¹⁴ to illuminate SiPMs with an incoherent light source. The light source utilized is a LED, model 430L from Thorlabs company [106], which gives an spectrum shown in Figure 3.18d. The spectrum was experimentaly measured with a spectrometer and fitted to a Gaussian function. It can be seen that the emission peak of this LED is placed at 436.3 with a FWHM¹⁵ of 19.1 nm. With the help of this LED we intend to simulate the light emission of the fibers of the TRITIUM experiment to calibrate the SiPMs at the working wavelength.

2. The second PCB, shown in Figure 3.18b, sums the different signals of the SiPMs and amplify them by a factor $G = 4187.5$ or $G = 10761.88$, depending on the input resistance of the oscilloscope, 50Ω or $1 M\Omega$, respectively. This PCB uses a differential amplification that reduce the electronic noise of the system and is connected to the first PCB through two HDMI feedthroughs.
3. The third PCB, shown in Figure 3.18c, rearranges all the different input and output signals in an HDMI connection to avoid crosstalk between different signals. This PCB is connected to the second PCB trough a HDMI feedthrough.

The input signals are the supply voltage of the SiPMs and the supply voltage of the PCBs (± 6 V) and the output signals are the temperature sensor signal and the summed signal of all SiPMs.

The output signal of the third PCB is connected to an oscilloscope, model ..., that records the data which are subsequently analized by ROOT¹⁶.

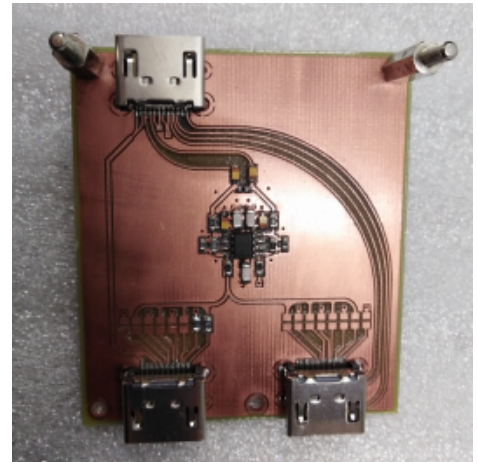
¹⁴The optical fiber used is BCF-98 from Saint-Gobain company [105]

¹⁵The FWHM parameter, Full Width at Half Maximum, of a Gaussian fit can be calculated from its sigma using the equation: $FWHM = 2.35 \cdot \sigma$

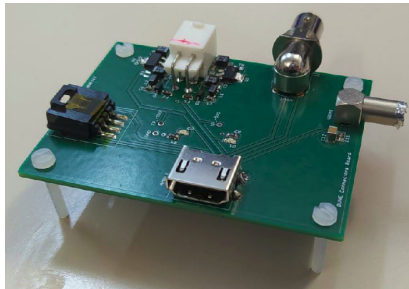
¹⁶ROOT is a framework for data processing, based on C ++ and object-oriented



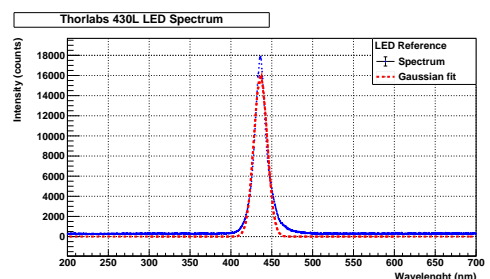
(a) PCB 1 used to arrange 8 SiPMs and black box.



(b) PCB 2 used to sum and amplify the output signals of SiPMs.



(c) PCB 3 used to rearrange the different signals of the system.



(d) Emission spectrum of the LED.

Figura 3.18 – Three PCBs used for the SiPM characterization and LED emission spectrum.

3.3 Ultrapure Water System

3.3.1 Introduction to the Ultrapure Water System

The objective of the ultrapure water system is to purify the water sample before the measurement. This system is essential is important for two reasons:

1. The mean free path of tritium electrons in water is around $5 \mu\text{m}$ and even less in solid materials like organic material. The electron from the tritium decay has to reach the fiber to be detected and, consequently, the detector must be kept very clean. If the analyzed water sample contains particles that may be deposited on the fibers, a layer of matter can be formed, preventing the tritium electrons from reaching the fibers and reducing drastically the tritium detection efficiency.
2. The tritium monitor does not have any spectrometric capabilities that can be used to distinguish other radioactive elements from tritium. That means that, any radioactive event in the analyzed water sample would be counted as a tritium event.

The ultrapure water system was designed to remove all particles up to a diameter of $1 \mu\text{m}$ and organic matter, which means that the only radioactive particle that passes through it is tritium.

In summary, the ultrapure water system is used to keep our detector clean, ensuring the stability of its detection efficiency and to eliminate all radioactive particles other than tritium.

technology, developed at CERN and widely used in nuclear and particle physics.

3.3.2 Set Up of Ultrapure Water System

The requirements of this water treatment device are:

- to obtain a high degree of purification of the processed water sample, reducing its conductivity by approximately two orders of magnitude (from $1000 \mu\text{S}/\text{cm}$ to $10 \mu\text{S}/\text{cm}$)
- to require of low maintenance (low cost and low manpower)
- to install a remote control device with probes and valves controlling by software.

The LARUEX laboratory in Extremadura, one of the six collaborators of the TRITIUM experiment, has designed, developed and built the ultrapure water system, a scheme of which is shown in Figure 3.19.

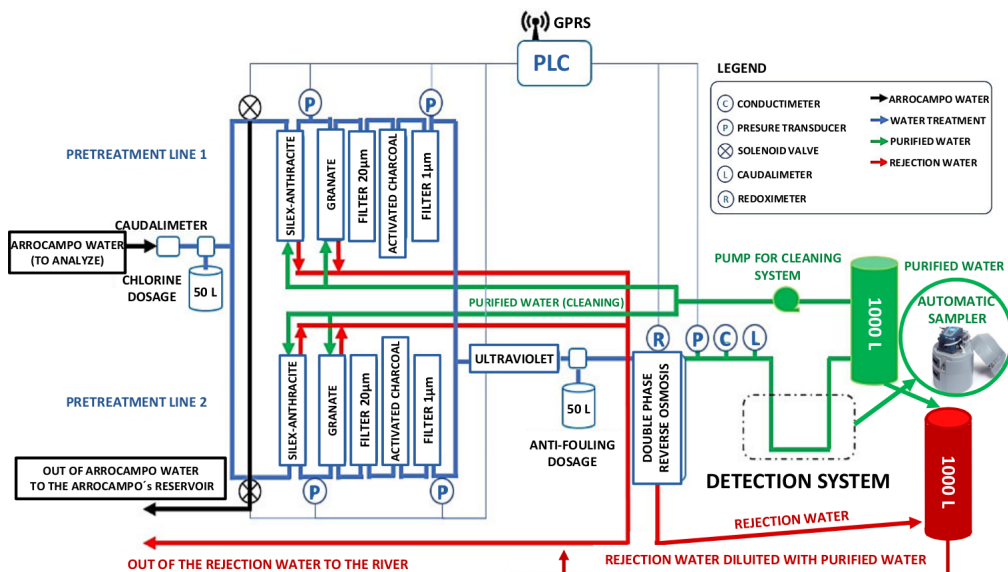


Figura 3.19 – Scheme of water purification system.

This system is installed in the Arrocampo dam and consists of four different consecutive stages:

1. The raw water from the Tagus River passes through two different filters, the first made of silex-anthracite and the second of garnet, with which a rough filtering is made (the largest particles are eliminated). This system has two parallel lines and implements self-cleaning by injecting ultrapure water in the opposite direction.
2. The outlet water sample of the first stage, called fine filtration stage, passes through a $20\text{ }\mu\text{m}$ filter (formed by a synthetic mesh) and activated charcoal filters (one per line) that removes chlorine and iron particles.
3. The outlet water of the second stage passes through a super-fine filtering consisting of a $1\text{ }\mu\text{m}$ filter, formed of a dense polypropylene mesh and UV lamps. The first filter removes all the particles up to diameters of $1\text{ }\mu\text{m}$ and the UV lamps remove the organic matter present in the sample.
4. Finally, the water is introduced in the last stage, double-phase reverse osmosis, that reduces the conductivity of the water to about $5\text{ }\mu\text{S}/\text{cm}$. It was verified that a conductivity of $10\text{ }\mu\text{S}/\text{cm}$ is achieved with only one module of reverse osmosis, enough for the needed conditions of tritium detector. Therefore, only one module of reverse osmosis is used for 24 h and the other, reducing the power consumption of the system.

As a result of the purification process, besides the ultrapure water that is introduced into TRITIUM detector, a rejection water, with conductivities greater than the original water containing the particles extracted from the ultrapure water is produced.

The ultrapure water system is able to process up to $0.850 \text{ m}^3/\text{h}$ with a single line operating or $1.480 \text{ m}^3/\text{h}$ with both, greatly overestimating the requirements of the tritium detector.

The software used for remote controlling of the ultrapure water system is Siemens PLC, that gives the information such as the state of the valves, the pressure probes or water production in real time.

The appendix B contains several pictures of different parts of this system, installed in Arrocampo dam.

3.4 Background Rejection System of TRITIUM Monitor

The objective of the background rejection system is to reduce the TRITIUM radioactive background. The TRITIUM project follows the ALARA principle for the tritium activity measurement, that is, to measure tritium activity "as low as reasonably achievable". The detection limit of tritium activity is set by the uncertainty in the activity of the radioactive background since tritium activities below this uncertainty cannot be distinguished from the background. Therefore, the background uncertainty must be reduced as much as possible.

The total uncertainty is a quadratic sum of all the different uncertainties related to the measurement, i. e., the statistical uncertainty¹⁷, σ_{st} , the systematic uncertainty¹⁸, σ_{si} .

The background rejection system of TRITIUM monitor minimizes the statistical component. Because of the Poissonian nature of the process,

¹⁷Uncertainty due to the statistical nature of the radioactivity process

¹⁸uncertainty due to the manufacture of the detectors

the statistical uncertainty corresponds to the square root of the measured activity, A_m , which can be reduced by minimizing detected background events.

$$\sigma_T^2 = \sigma_{st}^2 + \sigma_{si}^2; \quad \sigma_{st;bak} = \sqrt{A_{m;bak}} \quad (3.11)$$

The background of TRITIUM is due to natural radioactivity and has two different sources. On the one hand, radioactive elements that are present in the crust of Earth, mainly ^{40}K and elements from the four different natural radioactive series, shown in Table 3.4. On the other hand, the cosmic ray radiation. The primary cosmic radiation is composed of high-energy particles, mainly protons and α , but, after interacting with the Earth's atmosphere, they generate a shower mainly composed by muons, electrons, photons and neutrons mainly.

Mass Num.	Series	Prim. el.	Half life (y)	Final isotope
4n	Thorium	^{232}Th	$1.41 \cdot 10^{10}$	^{208}Pb
4n+1	Neptunium	^{237}Np	$2.14 \cdot 10^6$	^{209}Pb
4n+2	Uranium-Radium	^{238}U	$4.51 \cdot 10^9$	^{206}Pb
4n+3	Uranium-Actinium	^{235}U	$7.18 \cdot 10^8$	^{204}Pb

Table 3.4: Classification of natural radioactive series [107, 108].

Cosmic radiation depends on several parameter like the altitude and latitude of the Earth, the altitude, sea level in our case, and the solar activity cycle. The spatial distribution of cosmic rays, mainly muons, follows a $\cos^2(\theta)$ distribution with the zenith angle.

To remove the effect of background two different techniques are employed:

- On the one hand, the weak radiation, which is any radiation with

energy below 200 MeV/nucleon is stopped by a lead castle, described in section 3.4.1,

- On the other hand, the hard radiation, that is any radiation of energy greater than 200 MeV/nucleon, is much more difficult to stop and the technique used is a cosmic veto, reported in section 3.4.2 in anti-coincidence with the TRITIUM detector.

3.4.1 Passive Shield (Lead)

Weak radiation is suppressed by a lead shielding inside which the TRITIUM detector is placed. This lead shielding is effective for particle energies below 200 MeV/nucleon, which is due to the Earth's natural radioactivity and to the weak component of cosmic radiation. This lead shielding consists of 158 lead bricks with ultra-low intrinsic radioactivity, 25 mm thick. They are chevron shaped, shown in Figure 3.20a, specially designed for a perfect fit and easy assembly. As can be seen in Figures 3.20b and 3.20c, these lead bricks are arranged in two layers to a total thickness of 50 mm. The junction of the inner layer lead bricks is shielded by a lead brick of the outer layer to avoid any leak of radiation.

Special aluminum structure was designed by mechanical engineering department of CENBG, shown in Figure 3.21, to support the total weight of the lead bricks, 2.4 tons.

The internal room of the lead shielding is divided in two parts, as exhibited in Figure 3.20. The larger one has internal dimensions of $90.5 \cdot 41 \cdot 51$ cm³ and is used to place the TRITIUM detector. The smaller one, of dimensions of $33 \cdot 41 \cdot 51$ cm³, contains the DAQ system. The external dimensions of the lead shielding are $148 \cdot 60 \cdot 70$ cm³ and it weighs 2.5 tons.

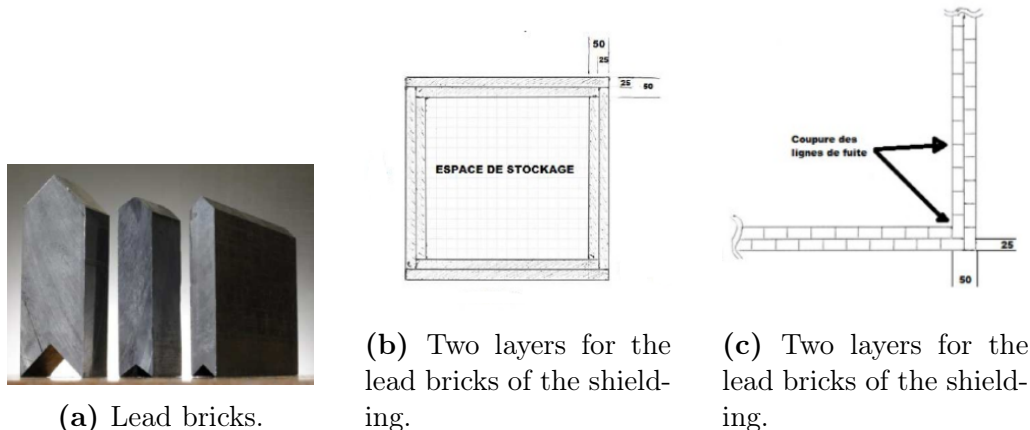


Figura 3.20 – Lead Bricks and their arrangement in the lead shielding.

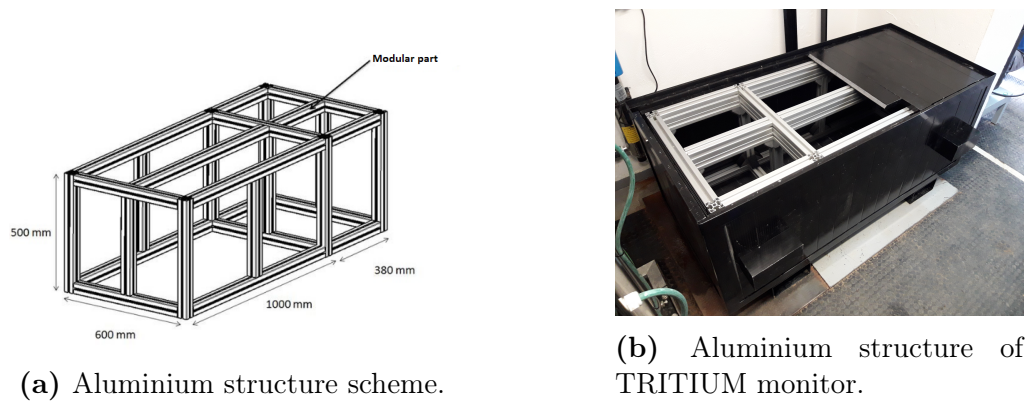


Figura 3.21 – Lead Bricks and their arrangement in the lead shielding.

3.4.2 Active Shield (Cosmic Veto)

As hard radiation cannot be stopped by a moderate lead thickness cosmic vetos are employed.

A cosmic veto consists of at least two complementary detectors in coincidence that reject simultaneous events in both.

As shown in Figure 3.22, the two complementary detectors were placed one above and the other below the TRITIUM detector. The distance between both detectors, 34.2 cm for our latest prototype developed, is set by the TRITIUM prototype to be placed between both.

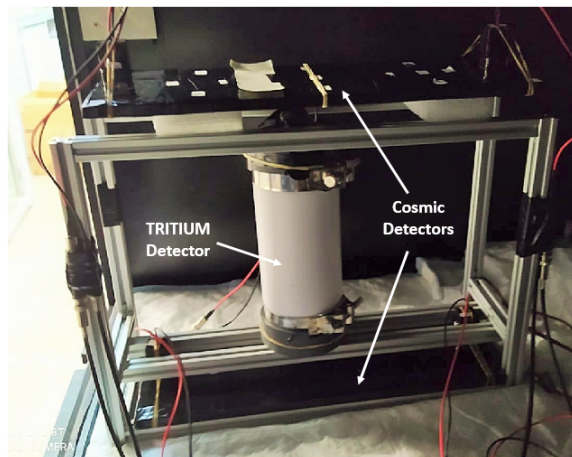


Figura 3.22 – Cosmic veto and Tritium-IFIC 2 prototype in an aluminum mechanical structure developed by IFIC’s mechanical engineering department.

A hard cosmic events simultaneous through both cosmic detectors is displayed in figure 3.23a. Each cosmic detector has two photosensors. Hard cosmic events are rejected when both detectors are in coincidence with the electronic configuration given in Figure 3.14c.

The TRITIUM detector is read out in anti-coincidence with the

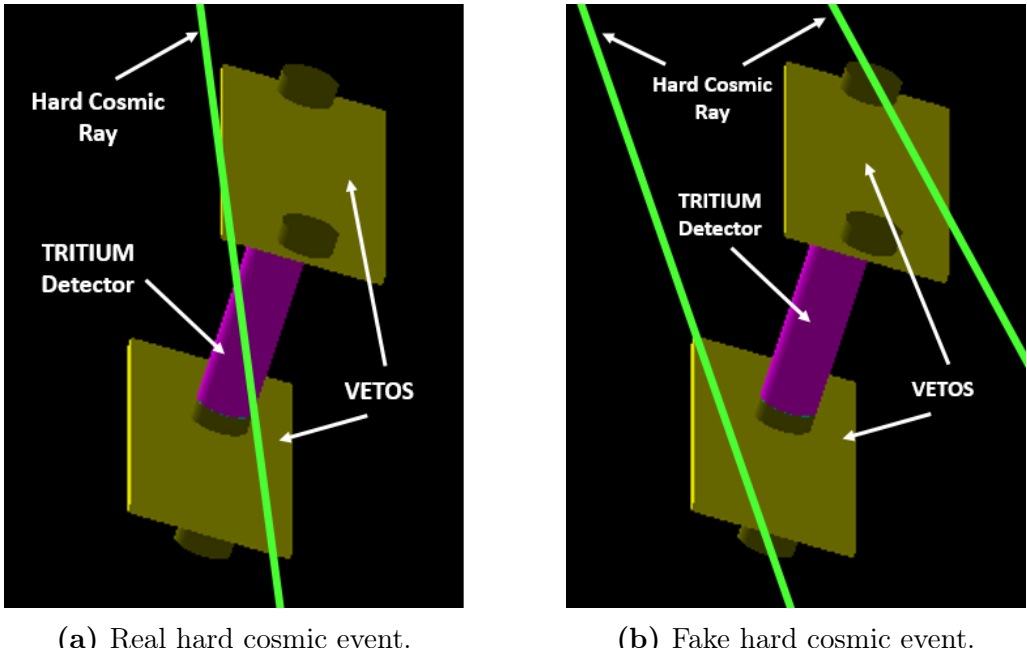


Figura 3.23 – Hard cosmic events detected with the cosmic veto of TRIUM: a) Affecting to the tritium measurement, b) Does not affecting to the tritium measurement.

cosmic veto. Random coincidence from cosmic two different hard cosmic events, one in each detector, shown in Figure 3.23b are negligible. The expected hard cosmic rate at sea level for muons, main contributor, is $70 \text{ m}^{-2}\text{s}^{-1}\text{sr}^{-1}$ [109, 110], that is $7^{-3} \text{ cm}^{-2}\text{s}^{-1}\text{sr}^{-1}$, shown in the cosmic rate plot of Figure 3.24. As time coincidences are triggered by logical gates of about 10 ns, the probability of recording two different hard cosmic events in temporal coincidence is less than 10^{-9} which is not worth considering.

The vetos are made of a plastic scintillator block from Epic-Crystal [112]. Its properties are given in Table 3.5 and its energy emission spectrum is displayed in Figure 3.25.

The energy spectrum has a peak very close to that of the scintillating fibers used, so the same photosensors are used to read out them. The

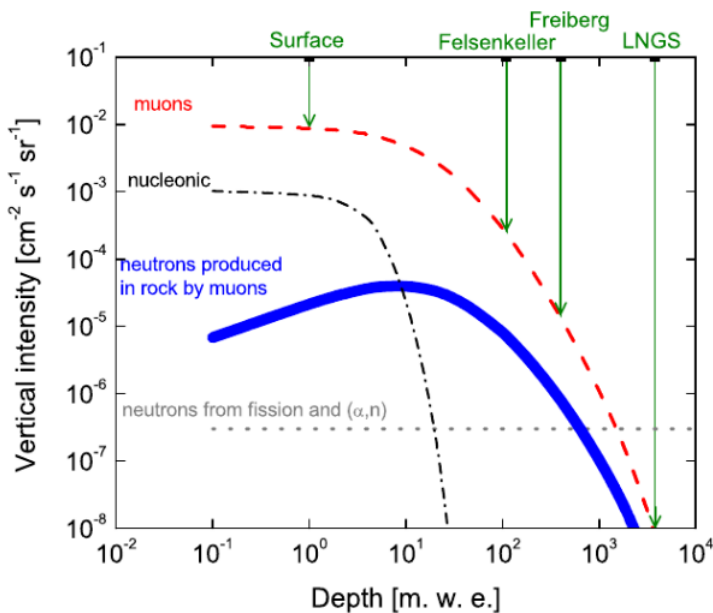


Figura 3.24 – Hard cosmic muon rate [111].

dimensions of the scintillator block are $45 \cdot 171 \text{ cm}^3$ and they are three foil wrapped by a layer of teflon, aluminum and black tape, exhibited in Figure 3.26. These layers prevent external photons from reaching the scintillator plastic and avoid photons generated by the scintillator plastic from escaping before reaching the photosensor. Two $2.5 \cdot 2.5 \text{ cm}^2$ windows are made on the wrapping to allow reading by the photosensors.

As previously mentioned, the expected hard cosmic rate at sea level is $7 \cdot 10^{-3} \text{ cm}^{-2}\text{s}^{-1}\text{sr}^{-1}$. As the solid angle of our detectors is $\omega = 0.5434$, calculated by integrating the solid angle of one scintillator on the other, and the area of the veto is 765 cm^2 , the expected hard cosmic rate on our cosmic vetos should be 2,909 event/s. Thus is important to determine the efficiency of the cosmic veto.

Base material	Polystyrene
Growth method	Polymeric
Density (g/cm ³)	1.05
Refractive index	1.58
Soften temperature (°)	75-80
Light output (Anthracene)	50-60%
H/C ratio	1.1
Emission peak (nm)	415 (Blue)
Decay Time, (ns)	2.4
Hygroscopic	No

Table 3.5: Properties of plastic scintillators from Epic-Crystals. [112]

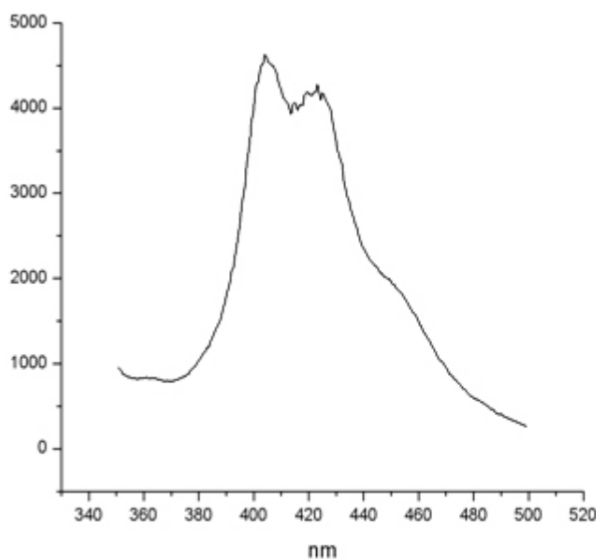


Figura 3.25 – Emission energy spectrum of the plastic scintillation used for the cosmic vetos. [112]

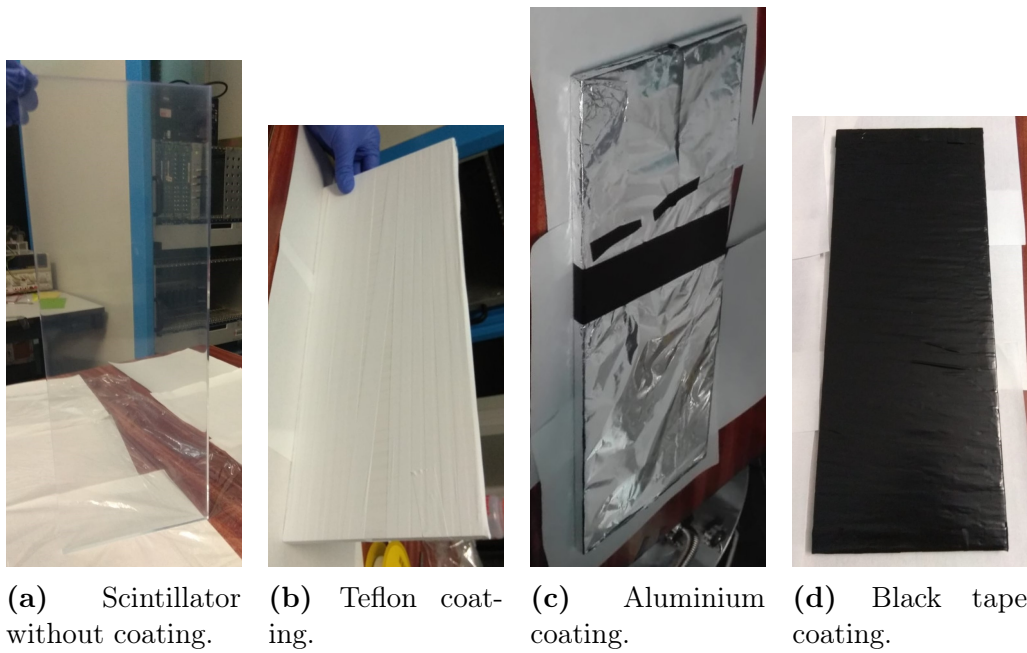


Figura 3.26 – Different layers used to cover of the cosmic veto.

Chapter 4

Research & Development on Detector Design and Components

4.1 Characterization and R&D on Scintillating Fibers

4.1.1 Scintillating Fiber Conditioning Process.

4.1.2 Automatic Polishing Machine for Scintillating Fibers

4.1.3 Characterization of Scintillating Fibers

Preparation of the System Used for the Characterization Study.

Results of the Characterization of Scintillating Fibers

4.1.4 Cleaning Process for Scintillating Fibers

4.2 Characterization and R&D on SiPM

Chapter 5

TRITIUM Monitor Prototypes

5.1 Preliminary IFIC prototypes, TRITIUM-IFIC 0 and TRITIUM-IFIC 1

5.1.1 TRITIUM-IFIC 0

5.1.2 TRITIUM-IFIC 1

5.2 Latest TRITIUM Prototypes

5.2.1 TRITIUM-Aveiro 0

5.2.2 Advanced IFIC prototype, Tritium-IFIC 2

5.3 Modular TRITIUM Detector for In-Situ Tritium Monitoring

Chapter 6

Simulations

6.1 Geant4 Environment

6.2 Description of the Simulations Performed

6.2.1 Tritiated Water Source

6.2.2 Energy deposition and light output of scintillating fibers

6.2.3 Fiber Length Optimization

6.2.4 Fiber Diameter Effect

6.2.5 Simulation of the Tritium-IFIC 2 Prototype

6.2.6 Simulation of the Lead Shielding and Cosmic Veto

Chapter 7

TRITIUM Monitor Results and Discussion

7.1 Results from Laboratory measurements

- 7.1.1 Experimental Results of TRITIUM-IFIC 0 Prototype
- 7.1.2 Experimental Results of TRITIUM-IFIC 1 Prototype
- 7.1.3 Experimental Results of TRITIUM-Aveiro 0 prototype
- 7.1.4 Experimental Results of TRITIUM-IFIC 2 prototype

7.2 Results from Measurements at Arrocampo dam

Chapter 8

Results of the TRITIUM Simulations

8.1 Optimization of the TRITIUM Monitor Design

8.1.1 Optimization of the Tritiated Water Source

8.1.2 Simulation of the Output Light of Scintillating Fibers

8.1.3 Optimization of the Scintillating Fiber Length

8.1.4 Optimization Scintillating Fiber Diameter

8.1.5 Effect of the PMMA windows

8.2 Simulation Results of TRITIUM monitor

Chapter 9

Conclusions and Prospects

Appendices

Appendix A

Electronical Schemes of PCBs Used for SiPM Characterization

Appendix B

Ultrapure Water System

Appendix C

Preparation of Liquid Radioactive Source of Tritium

98APPENDIX C. PREPARATION OF LIQUID RADIOACTIVE SOURCE OF TR

Appendix D

Electronic System of TRITIUM-Aveiro 0 prototype

Bibliography

- [1] IAEA, *The International Atomic Energy Agency Webpage*.
- [2] UNSCEAR, *The United Nations Scientific Committee on the Effects of Atomic Radiation Webpage*.
- [3] CSN, *Consejo de Seguridad Nuclear, Spain Webpage*.
- [4] ICRU, *International Commission of Radiological Units and Measurements Webpage*.
- [5] ICRP, *International Commission on Radiological Protection Webpage*.
- [6] ISR, *International Society of Radiology Webpage*.
- [7] UN, *United Nations Webpage*.
- [8] CSN, *Red de Estaciones Automáticas, REA Webpage*.
- [9] CSN, *Red de Estaciones de Muestreo, REM Webpage*.
- [10] *Council directive 2013/15/euratom*.
- [11] J. W. BERTHOLD, L. A. JEFFERS, *Phase 1 Final Report for In-Situ Tritium Beta Detector*, U. S. Department of Energy, McDermott Technology, Inc., Research and Development Division, **DE-AC21-96MC33128**, April, 1998.

- [12] J. W. BERTHOLD, L. A. JEFFERS, *In Situ Tritium Beta Detector*, U. S. Department of Energy, McDermott Technology, Inc. (MTI), Technology development data sheet, **DE-AC21-96MC33128**, May, 1999.
- [13] X- HOU, *Tritium and ^{14}C in the environmental and nuclear facilities: Sources and analytical methods*, Journal of the Nuclear Fuel Cycle and Waste Technology (JNFCWT), 16 (2018), 11-39 **DOI: 10.7733/jnfcwt.2018.16.1.11**.
- [14] REFERENCIAAAAAAAA.
- [15] *Avance del informe del sistema eléctrico español, 2019*, Red eléctrica española.
- [16] *China construirá 60 centrales nucleares en la próxima década*, Europa press.
- [17] *Inversión de EE. UU. de 35 millones para centrales nucleares*, Energy News
- [18] *Three mile island accident*, World Nuclear Association.
- [19] *International Energy Outlook 2013*. U. E. Energy Information Administration.
- [20] Tritium at Fermilab.
- [21] **Brookhaven National Laboratory (BNL)**.
- [22] ALEKSANDRA SAWODNI, ANNA PAZDUR, JACEK PAWLÝTA, *Measurements of Tritium Radioactivity in Surface Water on the Upper Silesia Region*, Journal on Methods and Applications of Absolute Chronology, Geochronometria, Vol. 18, pp 23-28 **2000**.
- [23] M. L. OLIPHANT, P. HARTECK and E. RUTHERFORD, *Transmutation Effects observed with Heavy Hydrogen*, Nature, 133, 413 (1934)**DOI: 10.1038/133413a0**.

- [24] LUIS W. ALVAREZ and R. CORNOG, *Helium and Hydrogen of Mass 3*, Physical Review Journals Archive, 56, 613 (1939) DOI: [10.1103/PhysRev.56.613](https://doi.org/10.1103/PhysRev.56.613).
- [25] *DOE Handbook: Primer on Tritium Safe Handling Practices*, U. S. Departament Of Energy Washington, D.C. 20585.
- [26] ROBERT HAIGHT, JOSEPH WERMER and MICHAEL FIKANI, *Tritium Production by Fast Neutrons on Oxygen: An Integral Experiment*, Journal of Nuclear Science and Technology, 39:sup2, 1232-1235, DOI: [10.1080/00223131.2002.10875326](https://doi.org/10.1080/00223131.2002.10875326).
- [27] INSTITUT DE RADIOPROTECTION ET DE SURETÉ NUCLÉAIRE *Tritium and the environment, Tritium and the environment*, IRSN, Enhancing nuclear safety.
- [28] , REFERENCIAAAA,
- [29] *International Atomic Energy Agency*.
- [30] *Tritium decay image*.
- [31] ZHANG LIN, *Simulation and Optimization Design of SiC-Basaed PN Betavoltaic Microbattery Using Tritium Source*, MDPI Open Access Journal 12/02/2020, DOI:[10.3390/cryst10020105](https://doi.org/10.3390/cryst10020105)
- [32] BLAUVELT, R.K., DEATON, M.R. and GILL, J.T., *Health Physics Manual of Good Practices for Tritium Facilities*, EG and G Mound Applied Technologies, Miamisburg, OH (United States), Technical Report, 01 December 1991, DOI: [10.2172/266889](https://doi.org/10.2172/266889).
- [33] TSUYOSHI MASUDA and TOSHITADA YOSHIOKA, *Estimation of radiation dose from ingested tritium in humans by administration of deuterium-labelled compounds and food*, Scientific reports, 02 February 2021, DOI: [10.1038/s41598-021-82460-5](https://doi.org/10.1038/s41598-021-82460-5).

- [34] Z. PIETRZAK-FLIS, I. RADWAN, Z. MAJOR and M. KOWALSKA, *Tritium Incorporation in Rats Chronically Exposed to Tritiated Food or Tritiated Water for Three Successive Generations*, Journal of Radiation Research, Vol 22, Issue 4, December 1981, page 434-442 DOI: [10.1269/jrr.22.434](https://doi.org/10.1269/jrr.22.434).
- [35] J.R. MARTIN and J.J. KORANDA, *Biological Half-Life Studies of Tritium in Chronically Exposed Knagaroo Rats*, Journal of Radiation Research, Vol 50, Issue 2, May 1972, page 426-440 PMID: **5025235**.
- [36] T STRAUME and A. L. CARSTEN, *Tritium radiobiology and relative biological effectiveness*, Health Physics, Vol. 65, Number 6, December 1993, DOI: [10.1097/00004032-199312000-00005](https://doi.org/10.1097/00004032-199312000-00005) .
- [37] RYTOEMAA, T., SALTEVO, J. and TOIVONEN, H., *Radiotoxicity of Tritium-Labelled Molecules*, International Atomic Energy Agency symposium, IAEA, Vienna: Biological Implications of Radionuclides Released from Nuclear Industries, INIS Vol. 11, INIS Issue. 13, Reference Number, 11535484, 1979.
- [38] INTERNATIONAL COMMISSION ON RADIOLOGICAL PROTECTION, ICRP, *Recommendations of the ICRP. Annals of the ICRP, 21(1.3), 1991a. 1990. Oxford, Pergamon Press (Publication 60)..*
- [39] WORLD HEALTH ORGANIZATION, WHO, *Guidelines for Drinking-Water Quality. Vol 1. Third Edition. Geneve, Switzerland, 2004.*
- [40] INTERNATIONAL COMMISSION ON RADIOLOGICAL PROTECTION, ICRP, *Age-dependent doses to members of the public from intake of radionuclides: Part 5. Compilation of ingestion and inhalation dose coefficients. Oxford, Pergamon Press (International Commission on Radiological Protection Publication 72), 1996.*
- [41] DÉPARTEMENT FÉDÉRAL DE L'INTÉRIEUR, DFI (FEDERAL DEPARTMENT OF THE INTERIOR), *Ordonnance du DFI sur les sub-*

stances étrangères et les composants dans les denrées alimentaires (817.021.23), 2006, Switzerland (in French).

- [42] ONTARIO MINISTRY OF THE ENVIRONMENT, *Ontario Drinking Water Objectives*. Toronto, Ontario, 1994.
- [43] QUÉBEC, *Résultats du programme de surveillance de l'environnement du site de Gentilly. Rapport annuel 2006*. Québec, Canada..
- [44] RUSSIA, *NRB-99 Radiation Safety Norms*, 2007.
- [45] AUSTRALIAN GOVERNMENT, NATIONAL HEALTH AND MEDICAL RESERCH COUNCIL and NATURAL RESOURCE MANAGEMENT MINISTERIAL COUNCIL, *AustralianDrinking Water Guideilnes 6*, National Water Quality Managment Strategy, Version 3.6, Updated March 2011.
- [46] NUCLEAR ENERGY AGENCY, NEA, *Radiation and Nuclear Safety Authority*, 1993. Radioactivity of Household Water. ST 12.3. Erweko Paintuote, Helsinki, Finland, 1994.
- [47] OFFICE OF ENVIRONMENTAL HEALTH HAZARD ASSESSMENT, OEHHA, *Public Health Goals for Chemicals in Drinking Water-Tritium*. OEHHA, California ENfironmental Protection Agency, California USA, September, 2007.
- [48] UNITED STATES ENVIRONMENTAL PROTECTION AGENCY, US EPA, *Drinking Water Requirements for States and Public Water Systems*, Radionuclides Rule, 1976.
- [49] INSTITUT DE RADIOPROTECTION ET DE SÛRETÉ NUCLÉAIRE, IRSN (RADIOPROTECTION AND NUCELAR SAFETY INSTITUTE), *Bilan de l'état radiologique de l'environnement français de 2015 à 2017*. France.

- [50] BUNDESAMT FÜR STRAHLENSCHUTZ, BMU (FEDERAL OFFICE FOR RADIATION PROTECTION), *Environmental Radioactivity and Radiation Exposure*, Annual Report, 2005, (Jahresbericht 2005). BMU, Bonn, Germany (in German).
- [51] CONSEJO DE SEGURIDAD NUCLEAR, CSN, NUCLEAR SAFETY COUNCIL, *National Regulation of Radionuclides*.
- [52] EUROPEAN ATOMIC ENERGY COMMUNITY, EURATOM, *Council directive 2013/15/euratom*, October, 2013. Laying down requirements for the protection of the health of the general public with regard to radioactive substances in water intended for human consumption.
- [53] M. N. AL-HADDAD, A. H. FAYOUMI and F. A. ABU-JARAD, *Calibration of a liquid scintillation counter to assess tritium levels in various samples*, Nuclear Instruments and Methods in Physics Research A, Volume 438, Issues 2-3, December 1999, Pages 356-361, DOI: [10.1016/S0168-9002\(99\)00272-7](https://doi.org/10.1016/S0168-9002(99)00272-7).
- [54] K. J. HOFSTETTER and H. T. WILSON, *Aqueous Effluent Tritium Monitor Development*, Fusion Technology, Volume 21, 2P2, Pages 446-451, March 1992, DOI: [10.13182/FST92-A29786](https://doi.org/10.13182/FST92-A29786).
- [55] M. PALOMO. A. PEÑALVER, C. AGUILAR and F. BORRULL, *Tritium activity levels in environmental water samples from different origins*, Applied Radiation and Isotopes, Volume 65, Issue 9, September 2007, Pages 1048-1056, DOI: [10.1016/j.apradiso.2007.03.013](https://doi.org/10.1016/j.apradiso.2007.03.013).
- [56] R. A. SIGG, J. E. McCARTY, R. R. LIVINGSTON and M. A. SANDERS, *Real-time aqueous tritium monitor using liquid scintillation counting*, FNuclear Instrument and Methods in Physics Research A, Volume 353, Issues 1-3, 30 Decembre 1994, Pages 494-498 DOI: [10.1016/0168-9002\(94\)91707-8](https://doi.org/10.1016/0168-9002(94)91707-8).
- [57] N. P. KHERANI, *An alternative approach to tritium-in-water monitoring*, Nuclear and Methods in PHysics Research A, Volume 484,

Issues 1-3, 21 May 2002, Pages 650-659 DOI: [10.1016/S0168-9002\(01\)02008-3](https://doi.org/10.1016/S0168-9002(01)02008-3)

- [58] Z. CHEN, S. PENG, D. MENG Y. HE and H. WANG, *Theoretical study of energy deposition in ionization chambers for tritium measurements*, Review of Scientific Instruments, 84, 103302, 2013, DOI: [10.1063/1.4825032](https://doi.org/10.1063/1.4825032).
- [59] C. G. ALECU, U. BESSERER, B. BORNSCHEIN, B. KLOPPE, Z. KÖLLÖ and J. WENDEL, *Reachable Accuracy and Precision for Tritium Measurements by Calorimetry at TLK*, Fusion Science and Technology, 60:3, 937-940, DOI: [10.13182/FST11-A12569](https://doi.org/10.13182/FST11-A12569).
- [60] A. BÜKKI-DEME, C. G. ALECU, B. KLOPPE and B. BORNSCHEIN, *First results with the upgraded TLK tritium calorimeter IGC-V0.5*, Fusion Engineering and Design, Volume 88, Issue 11, November 2013, Pages 2865-2869 DOI: [10.1016/j.fusengdes.2013.05.066](https://doi.org/10.1016/j.fusengdes.2013.05.066).
- [61] M. MATSUYAMA, Y. TORIKAI, M. HARA and K. WATANABE, *New Technique for non-destructive measurements of tritium in future fusion reactors*, IAEA Nuclear Fusion, Volume 47, Number 7, S464, June 2007, DOI: [10.1088/0029-5515/47/7/S09](https://doi.org/10.1088/0029-5515/47/7/S09).
- [62] M. MATSUYAMA, *Development of a new detection system for monitoring high-level tritiated water*, Fusion Engineering and Design, Volume 83, Issue 10-12, December 2008, Pages 1438-1441 DOI: [10.1016/j.fusengdes.2008.05.023](https://doi.org/10.1016/j.fusengdes.2008.05.023).
- [63] S. NIEMES, M. STURM, R. MICHLING and B. BORNSCHEIN, *High Level Tritiated Water Monitoring by Bremsstrahlung Counting Using a Silicon Drift Detector*, Fusion Science and Technology, 67:3, 507-510, 2015, DOI: [10.13182/FST14-T66](https://doi.org/10.13182/FST14-T66).
- [64] K. S. SHAH, P. GOTHSKAR, R. FARRELL and J. GORDON, *High Efficiency Detection of Tritium Using Silicon Avalanche Photodiodes*,

IEEE Transactions on Nuclear Science, Volume 44, Issue 3, June 1997,
DOI: 10.1109/23.603750

- [65] P. JEAN-BAPTISTE, E. FOURRÉ, A. DAPOIGNY, D. BAUMIER, N. BAGLAN and G. ALANIC, *³He mass spectrometry for very low-level measurement of organic tritium in environmental samples*, Journal of Environmental Radioactivity, Volume 101, Issue 2, February 2010, Pages 185-190, **DOI: https://doi.org/10.1016/j.jenvrad.2009.10.005**.
- [66] C. BRAY, A. PAILOUX and S. PLUMERI, *Tritiated water detection in the 2.17 μM spectral region by cavity ring down spectroscopy*, Nuclear Instruments and Methods in Physics Research A, Volume 789, 21 July 2015, Pages 43-49, **DOI: 10.1016/j.nima.2015.03.064**.
- [67] M. MURAMATSU, A. KOYANO and N. TOKANUGA, *A Scintillation Probe for Continuous Monitoring of Tritiated Water*, Nuclear Instruments and Methods, Volume 54, Issue 2, October 1967, Page 325-326, **DOI: 10.1016/0029-554X(67)90645-3**.
- [68] A. A. MOGHISSI, H. L. KELLEY, C. R. PHILLIPS and J. E. REGNIER, *A Tritium Monitor Based on Scintillation*, Nuclear Instruments and Methods, Volume 68, Issue 1, 1 February 1969, Page 159, **DOI: 10.1016/0029-554X(69)90705-8**.
- [69] R. V. OSBORNE, *Detector for Tritium in Water*, Nuclear Instruments and Methods, Volume 77, Issue 1, 1 January 1970, Page 170-172, **DOI: 10.1016/0029-554X(70)90596-3**.
- [70] A. N. SINGH, M. RATNAKARAN and K. G. VOHRA, *An Online Tritium-in-Water Monitor*, Nuclear Instruments and Methods, Volume 236, Issue 1, 1 May 1985, Page 159-164, **DOI: 10.1016/0168-9002(85)90141-X**.
- [71] M. RATNAKARAN, R. M. REVETKAR, R. K. SAMANT and M. C. ABANI, *A Real-time Tritium-In-Water Monitor for Measurement Of*

Heavy Water Leak To The Secondary Coolant, International congress of the International Radiation Protection Association, Volume 32, Issue 15, 14-19 May 2000, P-3a-197, Reference number: **32015986**

- [72] K. J. HOFSTETTER and H. T. WILSON, *Aqueous Effluent Tritium Monitor Development*, Fusion Technology, Volume 21, 2P2, 1992, Pages 446-451, **DOI: 10.13182/FST92-A29786**.
- [73] K. J. HOFSTETTER and H. T. WILSON, *Continuous Tritium Effluent Water Monitor at the Savannah River Site*, International conference on advances in liquid scintillation, Vienna (Austria), 14-18 September 1992.
- [74] *Tritium, Interreg Sudoe Program. Tritium website.*
- [75] CERN COLLABORATION, *Geant4: A toolkit for the simulation of the passage of particles through matter.. Website.*
- [76] GLENN F. KNOLL, *Radiation Detection and Measurement*, Third Edition, John Wiley and Sons, Inc. 1999.
- [77] WILLIAM R. LEO, *Techniques for Nuclear and Particle Physics Experiments: a how-to approach*, Second Revised Edition, Springer-Verlag Berlin Heidelberg GmbH, 1994. **DOI: 10.1007/978-3-642-57920-2**.
- [78] SAINT-GOBAIN CERAMICS AND PLASTICS, INC., *Scintillating Optical Fibers*, It's What's Inside that Counts, 2005-14. **Data sheet**.
- [79] , , .
- [80] , , .
- [81] HAMAMATSU PHOTONICS K.K., *Photonmultiplier tube R8520-406/R8520-506*. **Data sheet**.

- [82] JAVIER PÉREZ PÉREZ, *Caracterización de los Fotomultiplicadores R8520-06SEL para NEXT*, 25-06-2010.
- [83] DAVID LORCA GALINDO, *Tesis: SiPM based tracking for detector calibration in NEXT*, Departamento de física atómica, molecular y nuclear, Universidad de Valencia (UV), Valencia, Spain, 03/2015.
- [84] OSI OPTELECTRONICS, *Characteristics and Applications*.
- [85] HAMAMATSU PHOTONICS K.K. SOLID STATE DIVISION, *MPPC Multi-Pixel Photon Counter S13360-6050*. **Data sheet**.
- [86] HAMAMATSU PHOTONICS K.K. SOLID STATE DIVISION, *MPPC Multi-Pixel Photon Counter S13360-6075*. **Data sheet**.
- [87] HAMAMATSU PHOTONICS K.K. SOLID STATE DIVISION, *MPPC Multi-Pixel Photon Counter S13361-6050*. **Data sheet**.
- [88] HAMAMATSU PHOTONICS K.K. SOLID STATE DIVISION, *MPPC Multi-Pixel Photon Counter S13361-3050*. **Data sheet**.
- [89] SENSL SENSE LIGHT, *Introduction to the SPM TECHNICAL NOTE*. February 2017 **Document**.
- [90] KEITHLEY, A GREATER MEASURE OF CONFIDENCE, *Model 6487 Picoammeter/voltage source, Manual reference*. **Data sheet**.
- [91] TENNELEC, *Model TC 952 High Voltage Supply, Manual reference*. **Data sheet**.
- [92] WENZEL ELECTRONIK, *Model N 1330-4 High Voltage Power Supply*. **Website**.
- [93] PHILIPS SCIENTIFIC, *Model 740 Quad Linear Fan-In/Out, Manual reference*. **Data sheet**.
- [94] ORTEC, *Model 9326 FastPreamplifier, Manual reference*. **Data sheet**.

- [95] ORTEC, *Model 575A Amplifier, Manual reference. Data sheet.*
- [96] ORTEC, *Model 671 Spectroscopy Amplifier, Manual reference. Data sheet.*
- [97] ORTEC, *Model CF8000 Octal Constant-Fraction Discriminator, Manual reference. Data sheet.*
- [98] CAEN, *Model 84, 4 channels discriminator. Data sheet.*
- [99] LECROY, *Model 465 Coincidence Unit, Manual reference. Data sheet.*
- [100] CERN, *Coincidence Unit Type N6234, Manual reference. Data sheet.*
- [101] ORTEC, *Model 416A Gate and Delay Generator, Manual reference. Data sheet.*
- [102] AMPTEK, *MCA8000D, Pocket MCA, Digital Multichannel Analyzer, Manual reference. Data sheet.*
- [103] PETsys Electronics. **Website.**
- [104] Thorlabs, Inc.. **Website.**
- [105] SAINT-GOBAIN CERAMICS AND PLASTICS, INC., *Optical fiber BCF-98, Manual reference. Manual reference.*
- [106] THORLABS, *LED430L - 430 nm LED with a Glass Lens, 8 mW, TO-18. Datasheet.*
- [107] PALL THEODÓRSSON, *Measurement of weak radioactivity*, World Scientific, 1996.
- [108] R D EVANS, *The Atomic Nucleus*, McGraw-Hill, Inc., 1996.

- [109] P.A. ZYLA ET AL., (*Particle Data Grup*), *PDG, Prog. Theor. Exp. Phys.* **2020** no. 8, 083C01 (2020). **Website DOI:** [10.1093/ptep/ptaa104](https://doi.org/10.1093/ptep/ptaa104).
- [110] HIROYUKI SAGAWA & ITSUMASA URABE (2001), *Estimation of Absorbed Dose Rates in Air Based on Flux Densities of Cosmic Ray Muons and Electrons on the Ground Level in Japan*, *Journal of Nuclear Science and Technology*, 38:12, 1103-1108, **DOI:** [10.1080/18811248.2001.9715142](https://doi.org/10.1080/18811248.2001.9715142).
- [111] T. SZÜCS, D. BEMMERER, T. P. REINHARDT, K. SCHMIDT, M. P TAKÁCS, A. WAGNER, L. WAGNER, D. WEINBERGER AND K. ZUBER, *Cosmic-ray induced background intercomparison with actively shielded HPGe detectors at underground locations*. **DOI:** [10.1140/epja/i2015-15033-0](https://doi.org/10.1140/epja/i2015-15033-0).
- [112] EPIC CRYSTAL, *Plastic scintillator of Epic Crystal, Manual reference. Data sheet*.
- [113] THORLABS, *Guide to connectorization and polishing optical fibers*, 2006. **Manual Reference**.
- [114] INDISTROĀÑ FIBER OPTICAL, *POF Cutter block*. **Website**.
- [115] DAVID SÁEZ-RODRÍGUEZ, KRISTIAN NIELSEN, OLE BANG AND DAVID JOHN WEBB, *Simple Room Temperature Method for Polymer Optical Fibre Cleaving*, *Journal of lightwave technology*, vol 33, No. 23, December 1, 2015. **DOI:** [10.1109/JLT.2015.2479365](https://doi.org/10.1109/JLT.2015.2479365).
- [116] S.H. LAW, J.D. HARVEY, R.J. KRUHLAK, M. SONG, E. WU, G.W. BARTON, M.A. VAN EIJKELENBORG AND M.C.J. LARGE, *Cleaving of microstructured polymer optical fibres*. **DOI:** [10.1016/j.optcom.2005.08.011](https://doi.org/10.1016/j.optcom.2005.08.011).
- [117] NANOTEC, *ST4209S1404-A - STEPPER MOTOR NEMA 17*. **Data sheet**.

- [118] *ARDUINO*, **Website**.
- [119] *CNC shield V3.0, Reference manual*.
- [120] *ALLEGRO Driver Pololu A4988, DMOS Microstepping Driver with Translator And Overcurrent Protection, Data sheet*.
- [121] *TEXAS INSTRUMENTS Driver DRV8825 Stepper Motor Controller IC, Data sheet*.
- [122] *Driver TMC2208, Step/Dir Drivers for Two-Phase Bipolar Stepper Motors up to 2A peak- StealthChop for Quiet Movement- UART Interface Option, Data sheet*.
- [123] ROITHNER LASERTECHNIK GMBH *LED435-03, 20 mW, 20 mA, Reference*.
- [124] , , **Reference**.
- [125] SAINT-GOBAIN CERAMICS AND PLASTICS, INC., *BC-630, Silicone Optical Grease, Website*.
- [126] THORLABS, *BK5 - Black Nylon, Polyurethane-Coated Fabric, 5'x9' (1.5m x 2.7m) x 0.005" (0.12 mm) Thick, Datasheet*.
- [127] SAN NOPCO COMPANY, *Wetting property, Website*.
- [128] HANNA INSTRUMENTS, *Multiparamétrico con opciones GPS, sonda autoregistradora, turbidez e ISE, Website*.
- [129] CAEN COMPANY, *Quad Scaler And Preset Counter-Timer, N1145, Datasheet*.
- [130] PHYSIKALISCH-TECHNISCHE BUNDESANSTALT, PTB, BRAUNSCHWEIG AND BERLIN, GERMANY *Calibration Certificate of tritium source, PTB-6.11-2005-1442*.

- [131] SAINT-GOBAIN CERAMICS AND PLASTICS, INC., *Scintillating Optical Fibers*, It's What's Inside that Counts, 2005-14. **Data sheet**.
- [132] HAMAMATSU PHOTONICS K.K., *Photonmultiplier tube R2154-02 2"*. **Data sheet**.
- [133] HAMAMATSU PHOTONICS K.K., *High Voltage Power Supply C11152-01*. **Data sheet**.
- [134] MAXIM INTEGRATED, *Low-Power, Quad, 12-Bit, Voltage-Output DACs with Serial Interface*. **Data sheet**.
- [135] SAINT-GOBAIN, *Scintillating plastic grown with polymeric method*. **Data sheet**.
- [136] CREMAT INC., *CR 111-R2.1 Charge sensitive preamplifier*. **Data sheet**.
- [137] TEXAS INSTRUMENTS, *OPA656 Wideband, Unity-Gain Stable, FET-Input Operational Amplifier*. **Data sheet**.
- [138] LINEAR TECHNOLOGY, *LT111A*. **Data sheet**.
- [139] TEXAS INSTRUMENTS, *SN74AHC1G32 Single 2-Input Positive-OR Gate*. **Data sheet**.
- [140] TEXAS INSTRUMENTS, *SN74LVC1G11DBVR Single 3-Input Positive-AND Gate*. **Data sheet**.
- [141] J. ALLISON, *Geant4 - A simulation toolkit*. DOI:[10.1016/S0168-9002\(03\)01368-8](https://doi.org/10.1016/S0168-9002(03)01368-8)
- [142] PLOT NUCLEAR DATA (NADS), *Physics simulation packages, CRY (cosmic-ray particle showers)*. **Website**
- [143] CHRIS HAGMANN, DAVID LANGE and DOUGLAS WRIGHT, *Cosmic-Ray particle Showers Generator (CRY) for Monte Carlo*

- Transport Codes*, IEEE Nuclear Science Symposium conference record. Nuclear Science Symposium 2:1143-1146, January 2007. **DOI:10.1109/NSSMIC.2007.437209**
- [144] H. BUITEVELD, J.H.M. HAKVOORT, M. DONZE, *Optical properties of pure water*, in:*Proc. 2258 Ocean Optics XII, Bergen, Norway, 1994*. **DOI:10.1117/12.190060**
- [145] S. MAERTENS, ET AL., *Sensitivity of next-generation tritium beta-decay experiments for keV-scale sterile neutrinos*, *J. Cosmol. Astropart. Phys.* 2015 (2015) 020. DOI:10.1088/1475-7516/2015/02/020
- [146] J. ARGYRIADES, ET AL., *Spectral modeling of scintillator for the NEMO-3 and SuperNEMO detectors*, *Nucl.Instrum. Methods A* 625 (2011) 20-28. **DOI:10.1016/j.nima.2010.09.027**
- [147] J B BIRKS, *Scintillations from Organic Crystals: Specific Fluorescence and Relative Response to Different Radiations*, *Proc. Phy. Soc. A* 64 874, April 12th, 1951. **DOI:10.1088/0370-1298/64/10/303**
- [148] B.D. LEVERINGTON, M. ANELLI, P. CAMPANA and R. ROSELLINI, *A 1mm Scintillating Fibre Tracker Readout by a Multi-anode Photomultiplier*, July 5, 2011, arXiv.
- [149] CAEN, TOOLS FOR DISCOVERY, *CAEN V1724, 8 Channels, 14 bit, 100MS/s Digitalizer*. **Data sheet**
- [150] LLOYD, A. CURRIE, *Limits for Qualitative Detection and Quantitative Determination. Application to Radiochemistry*, *Anal. Chem.* 1968, 40, 3, 586-593, March 1, 1968. **DOI: 10.1021/ac60259a007**
- [151] C.D.R. AZEVEDO, A. BAEZA, E. CHAUVEAU, J.A. CORBACHO, J. DÍAZ, J. DOMANGE, C. MARQUET, M. MARTINEZ-ROIG, F. PIQUEMAL, J.F.C.A. VELOSO and N. YAHALALI, *First prototype module development for a tritium in water real-time monitor*.

- [152] C.D.R. AZEVEDO, A. BAEZA, E. CHAUVEAU, J.A. CORBACHO, J. DÍAZ, J. DOMANGE, C. MARQUET, M. MARTINEZ-ROIG, F. PIQUE-MAL, J.F.C.A. VELOSO and N. YAHLALI, *Simulation results of a real-time in water tritium monitor*, *Nuclear Instruments and Methods in Physics Research Section A: Accelerators, Spectrometers, Detectors and Associated Equipment*, Vol. 982, 1 December 2020, pages 164555. DOI: [10.1016/j.nima.2020.164555](https://doi.org/10.1016/j.nima.2020.164555)